tained from 136 primary neuroblastomas. The highly reliable statistical analysis by using a neuroblastoma proper cDNA microarray harboring 5340 genes based on an electrically controlled ceramics-based ink-jet method led us to design a cDNA microarray system harboring 200 genes, which is applicable to short-term (2 year) and long-term (5 year) prognosis predictions for neuroblastoma.

Our study demonstrated that the supervised classifier produced by the 5340 genes system provided a high accuracy (88.5%) for the 5 year outcome prediction, with a good balance between sensitivity (86.7%) and specificity (89.4%). Although age at diagnosis, disease stage, *MYCN* amplification, and patients found by mass screening have been useful prognostic markers currently used at the bedside, most of them have either high sensitivity or high specificity (Table 1). The microarray analysis showed the best sensitivity-specificity balance among the prognostic factors for predicting the outcome of neuroblastoma. When the classifier is combined with the age at diagnosis, the disease stage (stage 1, 2, or 4s versus stage 3 or 4) and the *MYCN* amplification, accuracy, sensitivity, and specificity increased up to 95.8%, 93.3%, and 97.0%, respectively. Furthermore, the intermediate subset of neuroblastomas (type II), for which a long-term prognosis is usually difficult to make, was also categorized by microarray analysis into groups of patients with a favorable prognosis and those with an unfavorable prognosis. These successful results led us to produce a more practical tool at the bedside, the mini-chip system, whose accuracy, sensitivity, and specificity were 87.8%, 76.5%, and 93.8%, respectively, when the classifier constructed by the 5340 genes system was applied to 50 independent samples measured by the mini-chip system, and were 91.8%, 82.4% and 96.9%, respectively, when another classifier was constructed by applying the LTO procedure to the same data (Figure 4).

It is well recognized now that gene expression analyses for cancer prognosis prediction should pay close attention to the reproducibility of obtained results. A complete crossvalidation analysis without introducing any information leakage and an independent test using new samples are necessary. Although the determination of the appropriate number of genes used in supervised classifiers should be included in the validation procedure, it has often been ignored in most microarray studies. van 't Veer et al. (2002) applied the supervised classification to the breast cancer gene signature, which is predictive of a short interval to distant metastases in 78 patients who were initially devoid of local lymph node metastasis. Although their crossvalidation analysis without the validation of the number of genes correctly predicted the actual outcome of disease for 63 of 78 patients (80.7%), the accuracy was worse when a complete validation was applied (73.1%). This difference suggests that even small information leakage may lead to overestimation of the accuracy. Beer et al. (2002) applied the supervised classification to the outcome prediction of lung adenocarcinoma. Their statistical analysis was complete without any information leakage. They did not report the prediction accuracy, but we estimated the accuracy to be about 70% from the data in their paper and found that the prediction by their supervised classifier was not very superior to that by existing prognosis markers. Iizuka et al. (2003) applied the supervised classification to the prediction of intrahepatic recurrence within 1 year after curative surgery for hepatocellular carcinoma patients. Although their predictor showed sufficiently high accuracy in an independent test with 27 samples, their crossvalidation procedure excluded the validation of the determination process of the number of optimum genes (steps 5 and 6 in their algorithm). The high crossvalidation accuracy of 100% may be an overestimation due to the information leakage.

According to the recent study that evaluated statistical methodologies used by microarray studies published between 1995 and April 2003, the three papers above were the only ones that reported both fairly sound crossvalidation analyses and independent tests (Ntzani and Ioannidis, 2003). Our LTO procedure includes the validation process of the number of genes used in the classifier and hence is a complete crossvalidation process. In addition, the obtained classifier was applied to the 50 independent samples that were measured by the reduced 200 genes system. This is a stronger test than usual independent tests but is important for the development of a practical system at the bedside. In addition, our LTO analysis achieved an almost unbiased estimation of the accuracy. Our crossvalidation analysis using the LTO procedure, the independent test of the classifier, and the validation of the procedure itself within a new experimental environment using the mini-chip system exhibited one of the most conservative and reliable statistical methodologies. In addition, our gene selection procedure according to the pairwise F score tries to extract correlation structures among genes, based on an idea similar to the exhaustive optimization method used in Iizuka et al. (2003), is beneficial in enhancing the applicability of the mini-chip system to various prediction problems, namely, short-term and long-term outcome predictions.

In addition to high accuracy, another advantage of our method is to provide a type of predictive information beyond the conventional binary prediction like favorable and unfavorable, which is ambiguous. The probabilistic output based on the hypothetical distribution obtained by the LTO analysis, the posterior probability, was found to show good accordance with actual survival rate (right bottom panel in Figure 2); this enables us to make a simple interpretation of the output: a patient with a posterior value of 0.8 has 80% chance for the 5 year survival, for example. Moreover, by calculating posterior probabilities for various future time points, a survival chance curve for each patient can be depicted (Figure 6). Although the follow-up period of patient "S057" is 2 years, and the patient is alive at this time, the individual survival chance curve says that his/her survival chance estimated from the gene expression pattern at diagnosis will get smaller than 50% at about 3 years after diagnosis. Such an individual survival chance curve can be used in choosing a suitable therapeutic protocol.

Another advantage of our method is that the probabilistic output is very stable in the presence of noise. Even when an artificial noise, whose variance is as large as the estimated noise variance of microarray, was added to expression profile data, prognosis prediction did not degrade very much (Figure S8). This robustness was confirmed when the noise variance went up to 1.0, which was sufficiently greater than the actual reproduction noise level of 0.4 (Figures S1A–S1C).

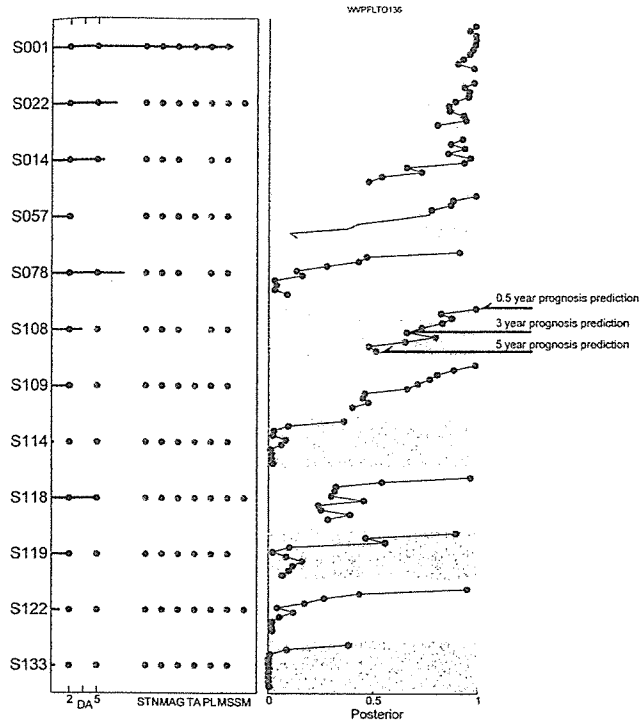

Figure 6. Individual survival chance analysis based on posterior probabilities

LTO estimation of survival probabilities at 0.5, 1.0, 1.5, ..., 5.0 years after diagnosis for 12 typical patients. Left panel: Information of patients (see caption of Figure 2). Right panel: Estimated posterior probabilities at 0.5, 1.0, 1.5, ..., 5.0 years after diagnosis, which predict the time course of patient's survival chance. A blue or a red mark denotes that the patient is alive or dead at that time after diagnosis, respectively. For example, the patient "S108," who died at 40 months, is predicted as 100% alive at 0.5 year and 52% alive at 5 year, solely from the microarray analysis at the diagnosis

The high outcome predictability of our system is attributable to multiple reasons. The quality of tumor samples is high because (1) an appropriate system was established for our neuroblastoma tissue bank, and (2) handling of tumor tissues is rather uniform at each hospital, in which informed consent was obtained. An array, produced by a new apparatus equipped with a piezo microceramic pump, generates highly reproducible signals. The noncontact spotting method makes the spot shape almost a perfect circle. Consequently, the spot excels in signal uniformity. We did not conduct microdissection of the 136 tumor samples, because the stromal components of the tumor, e.g., Schwannian cells, are already known to be very important to characterize its biology (Ambros and Ambros, 1995; Ambros and Ambros, 2000). Therefore, a good combination or selection of these procedures may have provided high outcome predictability. In addition, the high predictability was reliably confirmed by the complete crossvalidation analysis and the independent test. The probabilistic output based on the LTO analysis can provide a new type of information that will improve the therapeutic decision at the bedside. In addition, the probabilistic output is highly robust against noises that may be involved in test samples (described above); this can be the major reason for the high prediction accuracy when the classifier constructed by the 5340 genes system was applied to the data taken by the mini-chip system.

The impact of the selected genes is strong. The genes with the highest score in F group genes (F > UF) were *tubulin* α members (*TUBA3* and *K-ALPHA-1*, which corresponds to *TUBA1*), which have never been reported to be prognostic factors in neuroblastoma. Their prognostic significance has also been confirmed by RT-PCR in primary tumors (data not shown). The high expression of *TUBA1* in neuronal cells is associated with axonal outgrowth during development as well as with axonal degeneration after axotomy in adult animals (Knoops and Octave, 1997). The expression of *TUBA3* has been reported to be restricted to adherent, morphologically differentiated neuronal and glial cells (Hall and Cowan, 1985). We have also found that high expression of *tubulin tyrosine ligase* and enhanced tubulin tyrosination/detyrosination cycle are associated with neuronal differentiation in neuroblastomas with favorable prognosis (Kato et al., 2004). Thus, high mRNA expression of *TUBA* genes in favorable neuroblastoma may reflect differentiated status of tumors. ARHGEF7, Rho guanine nucleotide exchange factor 7, activates Rho proteins by exchanging bound GDP for GTP and can induce membrane ruffling. In our previous paper, we found that many family members of such G protein-related genes are highly expressed in favorable neuroblastomas compared to unfavorable ones (Ohira et al., 2003a). This may also imply a neuronal maturity nature of favorable tumors. Peripherin, a type III intermediate filament protein, was initially found as a cytoskeletal protein in the peripheral nervous system and in cultured cells of neuronal origin. This protein is known to be a marker of terminal neuronal differentiation; however, its functional role in neuroblastoma has been elusive. The previous evidence indicates that peripherin is transcriptionally upregulated by treatment with NGF, an important neurotrophin in neuroblastoma, and that the protein product is directly phosphorylated by NGF receptor, TrkA (Aletta et al., 1989). Thus, peripherin may play an important role as one of the signal transduction components involved in elaboration and maintenance of neuronal differentiation. In the UF gene group, many ribosomal protein-related genes are selected. *GNB2L1*, a receptor for activated C-kinase *RACK1*, is implicated in linking between *PKC* signaling and ribosome activation (Ceci et al., 2003). The *DDX1* gene, which is frequently coamplified with the *MYCN* gene in advanced neuroblastomas (Godbout and Squire, 1993; Noguchi et al., 1996), is also a member of this group. Its protein product is a putative RNA helicase and is implicated in a number of cellular processes involving alteration of RNA secondary structure such as translation initiation, nuclear and mitochondrial splicing, and ribosome and spliceosome assembly. *DDX1* is ranked at a higher score than the *MYCN* gene, which is concordant with the previous reports describing that *MYCN* mRNA expression is a weaker prognostic marker than its genomic amplification (Slavc et al., 1990). Another important prognostic factor, *TrkA*, is not included in the top 70 genes but in the 90 (in the top 20 genes when the 5 year label was used) (data not shown), probably due to its relatively low levels of mRNA expression as compared with those of other genes. The prognos-

tic effect of *TrkA* expression may be compensated by other genes which are affected or regulated by *TrkA* intracellular signaling. Similarly, *MYCN*-regulated genes such as ribosomal genes, translation initiation and elongation factors, and laminin receptor may compensate the effect of *MYCN* gene expression in aggressive tumors. It is intriguing that high mRNA expression of *p53* gene is also strongly related to unfavorable outcome. Although *p53* mutation is rare in primary neuroblastomas, and its gene product frequently accumulated in cytoplasm, an unknown mechanism that upregulates *p53* expression in aggressive tumors may exist.

Our results showed that the decision by majority by the genes selected based on microarray data alone can be a prognostic indicator comparative to the existing prognostic markers, and that the addition of the microarray data to the prognosis markers improved the outcome prediction (Table 1). The outcomes of patients belonging to the intermediate subset, whose prognosis prediction had been very difficult by existing prognosis markers, were effectively separated into favorable group and unfavorable group ($p < 10^{-4}$). The posterior value will help the decision of therapeutic modalities, and outcome prediction based on the posterior value is extremely robust against a possible noise. In addition, our practical, low-cost microarray carrying only 200 genes should make its clinical use possible. Our further validation by hybridizing RNA obtained from 50 fresh neuroblastomas on the 200 cDNAs microarray in a completely independent laboratory indicated that our prediction system is consistent and feasible. Therefore, the application of a highly qualified cDNA microarray at the bedside may bring tailored medicine that allows better treatment of neuroblastoma patients.

Experimental procedures

Patients and tumor specimens

Fresh, frozen tumor tissues were sent to the Division of Biochemistry, Chiba Cancer Center Research Institute, from a number of hospitals in Japan (1996–2002). Informed consent was obtained at each institution or hospital. We randomly selected tumor samples from this neuroblastoma tissue bank and then successfully conducted hybridization in 136 neuroblastomas consisting of 41 stage 1 tumors, 22 stage 2 tumors, 33 stage 3 tumors, 28 stage 4 tumors, and 12 stage 4s tumors. Among the 136 fresh neuroblastomas, seventeen tumors were obtained at the delayed primary surgery after giving chemotherapy, but the other 119 tumors were resected by biopsy or surgery without giving any therapy. After surgery, patients were treated according to the previously described common protocols (Kaneko et al., 1998). Biological information on each tumor, including *MYCN* gene copy number, *TrkA* gene expression, and DNA ploidy, was analyzed in our laboratory, as described previously (Hishiki et al., 1998). All the tumors were classified according to the International Neuroblastoma Staging System (INSS) (Brodeur et al., 1993). The stage 4s neuroblastoma shows a special pattern of clinical behaviors, and the tumor itself, as well as its widespread metastases to the skin, liver, or bone marrow, usually regresses spontaneously. For a better understanding of statistical results, we introduced Brodeur's classification of neuroblastoma subsets: type I (stages 1, 2, or 4s; a single copy of *MYCN*; blue marks in Figure 2), type II (stage 3 or 4; a single copy of *MYCN*; green marks in Figure 2), and type III (all stages; amplification of *MYCN*; red marks in Figure 2) (Brodeur and Nakagawara, 1992). Among 136 tumors that we analyzed, 66 were found by mass screening of urinary catecholamine metabolites at the age of 6 months, which has been performed nationwide in Japan from 1984 to 2004 (Sawada et al., 1984). The follow-up duration ranged between 3 and 241 months (median, 56 months; mean, 57.3 months) after diagnosis. All diagnoses of neuroblastoma were confirmed by the histological assessment of a surgically resected tumor specimen at each hospital. Shimada's classification (Shimada et al., 1984) was performed in 62 out of 136 cases. The macroscopic necroses in the tumor were excluded from the tissue sampling for molecular analysis. We used for the microarray analysis only the tumor samples whose adjacent tissues contained more than 70% tumor cells in the thin sections stained with hematoxylin-eosin. For independent test, 50 (19 were found by mass screening and 31 were clinically found) tumors (15 of stage 1, 6 of stage 2, 9 of stage 3, 14 of stage 4, and 6 of stage 4s) were used.

Total RNA was extracted from each frozen tissue according to the AGPC method (Chomczynski and Sacchi, 1987). RNA integrity, quality, and quantity were then assessed by electrophoresis on the Agilent RNA 6000 nanochip using Agilent 2100 BioAnalyzer (Agilent Technologies, Inc.).

cDNA microarray experiments

We previously obtained approximately 5,000 genes after selecting from 10,000 clones randomly picked up from the mixture of oligo-capping cDNA libraries, which were generated from three primary neuroblastomas with a favorable outcome (stage 1; high *TrkA* expression and a single copy of *MYCN*), three tumors with a poor prognosis (stage 3 or 4; low expression of *TrkA* and amplification of *MYCN*), and a stage 4s tumor (Ohira et al., 2003a; Ohira et al., 2003b). Using these isolated genes together with 80 known cDNAs that were thought to be neuroblastoma-related genes, we first constructed a neuroblastoma proper cDNA microarray (named CCC-NB5000-Chip) carrying 5340 cDNA spots (the 5340 genes system). Insert DNAs (average size, approximately 2.5kb) were amplified by polymerase chain reaction (PCR) from these cDNA clones, purified by ethanol precipitation, and spotted onto a glass slide at a high density with an ink-jet printing tool (NGK Insulators, Ltd.).

Ten micrograms each of total RNA were labeled with the CyScribe RNA labeling kit in accordance with the manufacturer's manual (Amersham Pharmacia Biotech), followed by probe purification with the Qiagen MinElute PCR purification kit (Qiagen). We used a mixture of equal amounts of RNA from each of four neuroblastoma cell lines (NB69, NBL-S, SK-N-AS, and SH-SY5Y) as a reference. RNAs extracted from primary neuroblastoma tissues and RNAs of the reference mixture were labeled with Cy3 and Cy5 dye, respectively, and were used as probes together with yeast tRNA and polyA for suppression. Subsequent hybridization and washing were conducted as described previously (Takahashi et al., 2002; Yoshikawa et al., 2000). Hybridized microarrays were scanned using the Agilent G2505A confocal laser scanner (Agilent Technologies, Inc.), and fluorescent intensities were quantified using the GenePix Pro microarray analysis software (Axon Instruments, Inc.). The procedure of this study was approved by the Institutional Review Board of the Chiba Cancer Center.

After selecting genes strongly related to the prognosis of patients with neuroblastoma (at 2 years and at 5 years after diagnosis), we constructed a 200 cDNAs microarray on glass slides by the same procedure described above (the mini-chip system). For the independent test using 50 samples, tumor RNA preparation, probe labeling, and hybridization were conducted in a completely different laboratory from the original 136 hybridization. In this independent test, 5 μg each of total RNA were used for labeling.

Data preprocessing

To remove chip-wise biases of a microarray system, we used the LOWESS normalization (Cleveland, 1979). When the Cy3 or Cy5 strength for a clone was smaller than 3, strength was regarded as abnormally small, and the log expression ratio of the corresponding clone was treated as a missing value. The rate of such missing entries was less than 1%. After normalizing the 5340 (genes) by 136 (samples) log expression matrix and removing missing values, each missing entry was imputed to an estimated value by Bayesian principal component analysis, which was developed previously (Oba et al., 2003).

Supervised machine learning and LTO crossvalidation

The 96 samples, whose prognosis at 5 years after diagnosis had been successfully checked, were used to train a supervised classifier that predicts the 5 year prognosis of a new patient. When we considered the short-term prediction, 126 samples whose 2 year prognosis is known were used. Selection of the genes that are related to the classification is an important preprocess for reliable prediction. We omitted the genes whose standard

deviation of the log ratios for the genes obtained over 136 experiments was smaller than 0.36, so that 1000 genes remained, because the background noise level was about 0.2–0.3. After the gene screening, the genes were scored by the pairwise *F* score, which is a modification of a pairwise correlation method (Bo and Jonassen, 2002), to conduct gene ranking in an attempt not only to obtain higher discrimination accuracy by using a smaller number of genes but also to reserve the applicability to various outcome prediction by the set of selected genes (see the Supplemental Data).

We used a well-established technique in the supervised classification (prognosis prediction), that is, weighted voting with linear discriminators, where each weight value was calculated as the signal-to-noise ratio (Golub et al., 1999). In the weighted voting, only n genes with the largest pairwise *F* score were used. The number of top genes, n, strongly affects the prediction accuracy (Figure S3) as found in various microarray studies and hence should be determined such to maximize the leave one out (LOO) crossvalidation accuracy. However, a naive determination process of n may introduce information leakage, and the accuracy optimized by the LOO crossvalidation involves overestimation. To avoid such an overestimation, we consulted a LTO analysis. The LTO analysis was constituted of inner and outer loops of LOO (Figure S2A); the gene number n was optimized by the LOO crossvalidation repeating the inner loops, and the optimized classifier was evaluated by an independent test for a single sample left out at a single step in the outer loop. During repetition of such steps, the test results of the outer loop were never fed back to the classifier's optimization process in the inner loops, and hence the tests in the outer loop did not include any overestimation, and the estimated accuracy involved the smallest bias as possible.

The posterior value for a single sample was calculated based on the distribution of the weighted vote (decision by majority by the genes that join the vote) *f* within the LTO analysis. We regard a real-valued weighted vote as carrying two kinds of information: its sign predicts the label (favorable or unfavorable) of the corresponding sample, and its absolute value shows the prediction strength. The posterior probability p for this sample being favorable (alive at 5 years) was evaluated as the logit transformation $p = \exp(\beta_0 + \beta_1 f)/[1 + \exp(\beta_0 + \beta_1 f)]$, where parameters β_0 and β_1 were estimated by the maximum likelihood method, in each step in the outer loop of LTO using the remaining 95 samples and the corresponding labels (5 year prognosis). Then, the posterior probability of the sample left out in the outer loop was predicted by the weighted vote *f* by the classifier constructed in the inner LOO loops and the parameters β_0 and β_1 obtained above. There is therefore no information leakage in this calculation process of the posterior of the sample left out.

Independent test

Using the 50 independent samples, we performed two kinds of tests. The first one is an independent test to validate the classifier obtained by our method and the applicability of our classifier to the mini-chip system, which has been developed as a clinical tool at the bedside (Figure S2B). According to the LTO analysis, the supervised classifier was finally constructed by using all of the 96 training samples measured by the 5340 genes system. This classifier was evaluated by being directly applied to the 50 samples measured by the mini-chip system without any information from measurements by the mini-chip system and the 50 test samples. In this test, tumor RNA preparation, probe labeling, and hybridization were conducted in a completely different laboratory from that for the 5340 genes system. The second one is to validate the LTO analysis to construct a supervised classifier by applying the procedure to the data taken by the mini-chip system.

Survival analysis

The Kaplan-Meier survival analysis was also programmed and used to compare patient survival. To assess the association of selected gene expression with patient clinical outcome, the statistical p and q values were calculated based on the log rank test.

Immunohistochemistry

Immunostaining with the antibody against peripherin protein (Santa Cruz Biotechnology; 1:400) was performed on six human neuroblastoma tumors selected from the surgical pathology file at the Department of Pathology, Aichi Medical University. They were all neuroblastoma (Schwannian stroma–poor) and included three favorable histology tumors (poorly differentiated subtype without *MYCN* amplification [one case]; differentiated subtype without *MYCN* amplification [two cases]) and three unfavorable histology tumors (undifferentiated subtype without *MYCN* amplification [one case]; poorly differentiated subtype with *MYCN* amplification [one case]; poorly differentiated subtype without *MYCN* amplification). All tumor tissues were obtained prior to chemotherapy and irradiation therapy. Four micron thick sections from the formalin-fixed, paraffin-embedded samples of these tumors were treated according to the protocol described previously (Kato et al., 2004). As for the negative controls, normal goat immunoglobulins (1:500 dilution; Vector Laboratories) were applied as the primary antibody.

Supplemental data

The Supplemental Data include Supplemental Experimental Procedures and ten supplemental figures and can be found with this article online at http://www.cancercell.org/cgi/content/full/7/4/337/DC1/.

Acknowledgments

We are grateful to the hospitals and institutions that provided us with surgical specimens (see the Supplemental Data). We also thank Shigeru Sakiyama and John K. Cowell for reading the manuscript; Naohiko Seki, Tsutomu Yoshikawa, and Masaki Kato for their valuable suggestions; and Natsue Kitabayashi, Tomonori Saito, Naoko Sugimitsu, Yuki Nakamura, Naoko Shibano, Emiko Kojima, Hisae Murakami, and Kazumi Yagyu for their technical support. This work was supported in part by a fund from Hisamitsu Pharmaceutical Co., Inc.; by Grants-in-Aid for Scientific Research on Priority Areas (C) "Medical Genome Science" and "Genome Information Science" and for Scientific Research (B) from the Ministry of Education, Culture, Sports, Science and Technology of Japan; and by Grant-in Aid for Cancer Research from the Ministry of Health, Labor and Welfare of Japan.

Received: November 17, 2003
Revised: January 8, 2005
Accepted: March 11, 2005
Published: April 18, 2005

References

Aletta, J.M., Shelanski, M.L., and Greene, L.A. (1989). Phosphorylation of the peripherin 58-kDa neuronal intermediate filament protein. J. Biochem. (Tokyo) *264*, 4619–4627.

Ambros, I.M., and Ambros, P.F. (1995). Schwann cells in neuroblastoma. Eur. J. Cancer *4*, 429–434.

Ambros, I.M., and Ambros, P.F. (2000). The role of Schwann cells in neuroblastoma. In Neuroblastoma, G.M. Brodeur, T. Sawada, Y. Tsuchida, and P.A. Voute, eds. (Amsterdam: Elsevier), pp. 229–243.

Beer, D.G., Kardia, S.L., Huang, C.C., Giordano, T.J., Levin, A.M., Misek, D.E., Lin, L., Chen, G., Gharib, T.G., Thomas, D.G., et al. (2002). Gene-expression profiles predict survival of patients with lung adenocarcinoma. Nat. Med. *8*, 816–824.

Berwanger, B., Hartmann, O., Bergmann, E., Bernard, S., Nielsen, D., Krause, M., Kartal, A., Flynn, D., Wiedemeyer, R., Schwab, M., et al. (2002). Loss of a FYN-regulated differentiation and growth arrest pathway in advanced stage neuroblastoma. Cancer Cell *2*, 377–386.

Bo, T., and Jonassen, I. (2002). New feature subset selection procedures for classification of expression profiles. Genome Biol. *3*, RESEARCH0017.

Bolande, R.P. (1974). The neurocristopathies: a unifying concept of disease arising in neural crest maldevelopment. Hum. Pathol. *5*, 409–429.

Brodeur, G.M., and Nakagawara, A. (1992). Molecular basis for clinical heterogeneity in neuroblastoma. Am. J. Pediatr. Hematol. Oncol. *14*, 111–116.

Brodeur, G.M., Seeger, R.C., Schwab, M., Varmus, H.E., and Bishop, J.M.

(1984). Amplification of N-myc in untreated human neuroblastomas correlates with advanced disease stage. Science *224*, 1121–1124.

Brodeur, G.M., Fong, C.T., Morita, M., Griffith, R., Hayes, F.A., and Seeger, R.C. (1988). Molecular analysis and clinical significance of N-myc amplification and chromosome 1p monosomy in human neuroblastomas. Prog. Clin. Biol. Res. *271*, 3–15.

Brodeur, G.M., Pritchard, J., Berthold, F., Carlsen, N.L., Castel, V., Castelberry, R.P., De Bernardi, B., Evans, A.E., Favrot, M., Hedborg, F., et al. (1993). Revisions of the international criteria for neuroblastoma diagnosis, staging, and response to treatment. J. Clin. Oncol. *11*, 1466–1477.

Ceci, M., Gaviraghi, C., Gorrini, C., Sala, L.A., Offenhauser, N., Marchisio, P.C., and Biffo, S. (2003). Release of eIF6 (p27BBP) from the 60S subunit allows 80S ribosome assembly. Nature *426*, 579–584.

Chomczynski, P., and Sacchi, N. (1987). Single-step method of RNA isolation by acid guanidinium thiocyanate-phenol-chloroform extraction. Anal. Biochem. *162*, 156–159.

Cleveland, W.S. (1979). Robust locally weighted regression and smoothing scatterplots. J. Am. Stat. Assoc. *74*, 829–836.

Evans, A.E., D'Angio, G.J., and Randolph, J. (1971). A proposed staging for children with neuroblastoma. Children's cancer study group A. Cancer *27*, 374–378.

Favrot, M.C., Combaret, V., and Lasset, C. (1993). CD44—a new prognostic marker for neuroblastoma. N. Engl. J. Med. *329*, 1965.

Godbout, R., and Squire, J. (1993). Amplification of a DEAD box protein gene in retinoblastoma cell lines. Proc. Natl. Acad. Sci. USA *90*, 7578–7582.

Golub, T.R., Slonim, D.K., Tamayo, P., Huard, C., Gaasenbeek, M., Mesirov, J.P., Coller, H., Loh, M.L., Downing, J.R., Caligiuri, M.A., et al. (1999). Molecular classification of cancer: class discovery and class prediction by gene expression monitoring. Science *286*, 531–537.

Hall, J.L., and Cowan, N.J. (1985). Structural features and restricted expression of a human α-tubulin gene. Nucleic Acids Res. *13*, 207–223.

Hishiki, T., Nimura, Y., Isogai, E., Kondo, K., Ichimiya, S., Nakamura, Y., Ozaki, T., Sakiyama, S., Hirose, M., Seki, N., et al. (1998). Glial cell line-derived neurotrophic factor/neurturin-induced differentiation and its enhancement by retinoic acid in primary human neuroblastomas expressing c-Ret, GFR α-1, and GFR α-2. Cancer Res. *58*, 2158–2165.

Hiyama, E., Hiyama, K., Yokoyama, T., Matsuura, Y., Piatyszek, M.A., and Shay, J.W. (1995). Correlating telomerase activity levels with human neuroblastoma outcomes. Nat. Med. *1*, 249–255.

Iizuka, N., Oka, M., Yamada-Okabe, H., Nishida, M., Maeda, Y., Mori, N., Takao, T., Tamesa, T., Tangoku, A., Tabuchi, H., et al. (2003). Oligonucleotide microarray for prediction of early intrahepatic recurrence of hepatocellular carcinoma after curative resection. Lancet *361*, 923–929.

Kaneko, M., Nishihira, H., Mugishima, H., Ohnuma, N., Nakada, K., Kawa, K., Fukuzawa, M., Suita, S., Sera, Y., and Tsuchida, Y. (1998). Stratification of treatment of stage 4 neuroblastoma patients based on N-myc amplification status. Study Group of Japan for Treatment of Advanced Neuroblastoma, Tokyo, Japan. Med. Pediatr. Oncol. *31*, 1–7.

Kato, C., Miyazaki, K., Nakagawa, A., Ohira, M., Nakamura, Y., Ozaki, T., Imai, T., and Nakagawara, A. (2004). High expression of human tubulin tyrosine ligase and enhanced tubulin tyrosination/detyrosination cycle are associated with neuronal differentiation in neuroblastomas with favorable prognosis. Int. J. Cancer *112*, 365–375.

Knoops, B., and Octave, J.N. (1997). α1-tubulin mRNA level is increased during neurite outgrowth of NG 108-15 cells but not during neurite outgrowth inhibition by CNS myelin. Neuroreport *8*, 795–798.

Look, A.T., Hayes, F.A., Nitschke, R., McWilliams, N.B., and Green, A.A. (1984). Cellular DNA content as a predictor of response to chemotherapy in infants with unresectable neuroblastoma. N. Engl. J. Med. *311*, 231–235.

Look, A.T., Hayes, F.A., Shuster, J.J., Douglass, E.C., Castleberry, R.P., Bowman, L.C., Smith, E.I., and Brodeur, G.M. (1991). Clinical relevance of tumor cell ploidy and N-myc gene amplification in childhood neuroblastoma: a Pediatric Oncology Group study. J. Clin. Oncol. *9*, 581–591.

Nagata, T., Takahashi, Y., Asai, S., Ishii, Y., Mugishima, H., Suzuki, T., Chin, M., Harada, K., Koshinaga, S., and Ishikawa, K. (2000). The high level of hCDC10 gene expression in neuroblastoma may be associated with favorable characteristics of the tumor. J. Surg. Res. *92*, 267–275.

Nakagawara, A., Arima, M., Azar, C.G., Scavarda, N.J., and Brodeur, G.M. (1992). Inverse relationship between trk expression and N-myc amplification in human neuroblastomas. Cancer Res. *52*, 1364–1368.

Nakagawara, A., Arima-Nakagawara, M., Scavarda, N.J., Azar, C.G., Cantor, A.B., and Brodeur, G.M. (1993). Association between high levels of expression of the TRK gene and favorable outcome in human neuroblastoma. N. Engl. J. Med. *328*, 847–854.

Nakagawara, A., Milbrandt, J., Muramatsu, T., Deuel, T.F., Zhao, H., Cnaan, A., and Brodeur, G.M. (1995). Differential expression of pleiotrophin and midkine in advanced neuroblastomas. Cancer Res. *55*, 1792–1797.

Noguchi, T., Akiyama, K., Yokoyama, M., Kanda, N., Matsunaga, T., and Nishi, Y. (1996). Amplification of a DEAD box gene (DDX1) with the MYCN gene in neuroblastomas as a result of cosegregation of sequences flanking the MYCN locus. Genes Chromosomes Cancer *15*, 129–133.

Ntzani, E.E., and Ioannidis, J.P. (2003). Predictive ability of DNA microarrays for cancer outcomes and correlates: an empirical assessment. Lancet *362*, 1439–1444.

Oba, S., Takemasa, N., Monden, M., Matsubara, K., and Ishii, S. (2003). A Bayesian missing value estimation method. Bioinformatics *19*, 2088–2096.

Ohira, M., Morohashi, A., Inuzuka, H., Shishikura, T., Kawamoto, T., Kageyama, H., Nakamura, Y., Isogai, E., Takayasu, H., Sakiyama, S., et al. (2003a). Expression profiling and characterization of 4200 genes cloned from primary neuroblastomas: identification of 305 genes differentially expressed between favorable and unfavorable subsets. Oncogene *22*, 5525–5536.

Ohira, M., Morohashi, A., Nakamura, Y., Isogai, E., Furuya, K., Hamano, S., Machida, T., Aoyama, M., Fukumura, M., Miyazaki, K., et al. (2003b). Neuroblastoma oligo-capping cDNA project: toward the understanding of the genesis and biology of neuroblastoma. Cancer Lett. *197*, 63–68.

Sawada, T., Hirayama, M., Nakata, T., Takeda, T., Takasugi, N., Mori, T., Maeda, K., Koide, R., Hanawa, Y., Tsunoda, A., et al. (1984). Mass screening for neuroblastoma in infants in Japan. Interim report of a mass screening study group. Lancet *2*, 271–273.

Schwab, M., Alitalo, K., Klempnauer, K.H., Varmus, H.E., Bishop, J.M., Gilbert, F., Brodeur, G., Goldstein, M., and Trent, J. (1983). Amplified DNA with limited homology to myc cellular oncogene is shared by human neuroblastoma cell lines and a neuroblastoma tumour. Nature *305*, 245–248.

Shimada, H., Chatten, J., Newton, W.A., Sachs, N., Hamoudi, A.B., Chiba, T., Marsden, H.B., and Misugi, K. (1984). Histopathologic prognostic factors in neuroblastic tumors; definition of subtypes of ganglioneuroblastoma and an age-linked classification of neuroblastomas. J. Natl. Cancer Inst. *73*, 405–416.

Shimono, R., Matsubara, S., Takamatsu, H., Fukushige, T., and Ozawa, M. (2000). The expression of cadherins in human neuroblastoma cell lines and clinical tumors. Anticancer Res. *20*, 917–923.

Slavc, I., Ellenbogen, R., Jung, W.H., Vawter, G.F., Kretschmar, C., Grier, H., and Korf, B.R. (1990). myc gene amplification and expression in primary human neuroblastoma. Cancer Res. *50*, 1459–1463.

Storey, J.D., and Tibshirani, R. (2003). Statistical significance for genome-wide studies. Proc. Natl. Acad. Sci. USA *100*, 9440–9445.

Takahashi, M., Seki, N., Ozaki, T., Kato, M., Kuno, T., Nakagawa, T., Watanabe, K., Miyazaki, K., Ohira, M., Hayashi, S., et al. (2002). Identification of the p33(ING1)-regulated genes that include cyclin B1 and proto-oncogene DEK by using cDNA microarray in a mouse mammary epithelial cell line NMuMG. Cancer Res. *62*, 2203–2209.

Ueda, K. (2001). Detection of the retinoic acid-regulated genes in a RTBM1 neuroblastoma cell line using cDNA microarray. Kurume Med. J. *48*, 159–164.

van 't Veer, L.J., Dai, H., van de Vijver, M.J., He, Y.D., Hart, A.A., Mao, M., Peterse, H.L., van der Kooy, K., Marton, M.J., Witteveen, A.T., et al. (2002). Gene expression profiling predicts clinical outcome of breast cancer. Nature *415*, 530–536.

Yamanaka, Y., Hamazaki, Y., Sato, Y., Ito, K., Watanabe, K., Heike, T., Nakahata, T., and Nakamura, Y. (2002). Maturational sequence of neuroblastoma revealed by molecular analysis on cDNA microarrays. Int. J. Oncol. *21*, 803–807.

Yoshikawa, T., Nagasugi, Y., Azuma, T., Kato, M., Sugano, S., Hashimoto, K., Masuho, Y., Muramatsu, M., and Seki, N. (2000). Isolation of novel mouse genes differentially expressed in brain using cDNA microarray. Biochem. Biophys. Res. Commun. *275*, 532–537.

Accession numbers

Microarray data are available at NCBI Gene Expression Omnibus (accession number GSE2283).

LMO3 Interacts with Neuronal Transcription Factor, HEN2, and Acts as an Oncogene in Neuroblastoma

Mineyoshi Aoyama,[1] Toshinori Ozaki,[1] Hiroyuki Inuzuka,[1] Daihachiro Tomotsune,[3] Junko Hirato,[4] Yoshiaki Okamoto,[1] Hisashi Tokita,[2] Miki Ohira,[1] and Akira Nakagawara[1]

Divisions of [1]Biochemistry and [2]Animal Science, Chiba Cancer Center Research Institute; [3]Center for Functional Genomics, Hisamitsu Pharmaceutical Co., Inc., Chiba, Japan and [4]Department of Pathology, Gunma University School of Medicine, Gunma, Japan

Abstract

LIM-only proteins (LMO), which consist of LMO1, LMO2, LMO3, and LMO4, are involved in cell fate determination and differentiation during embryonic development. Accumulating evidence suggests that LMO1 and LMO2 act as oncogenic proteins in T-cell acute lymphoblastic leukemia, whereas LMO4 has recently been implicated in the genesis of breast cancer. However, little is known about the role of LMO3 in either tumorigenesis or development. In the present study, we have identified *LMO3* and *HEN2*, which encodes a neuronal basic helix-loop-helix protein, as genes whose expression levels were higher in unfavorable neuroblastomas compared with those of favorable tumors. Immunoprecipitation and immunostaining experiments showed that LMO3 was associated with HEN2 in mammalian cell nucleus. Human neuroblastoma SH-SY5Y cells stably overexpressing LMO3 showed a marked increase in cell growth, a promotion of colony formation in soft agar medium, and a rapid tumor growth in nude mice compared with the control transfectants. More importantly, the increased expression of LMO3 and HEN2 was significantly associated with a poor prognosis in 87 primary neuroblastomas. These results suggest that the deregulated expression of neuronal-specific LMO3 and HEN2 contributes to the genesis and progression of human neuroblastoma in a lineage-specific manner. (Cancer Res 2005; 65(11): 4587-97)

Introduction

The LIM domain–containing proteins are important regulators in determining cell fate and controlling cell growth and differentiation during embryonic development (1). The LIM domain is a highly conserved cysteine-rich zinc finger–like motif found in a variety of nuclear and cytoplasmic proteins and acts as a docking site for the assembly of multiprotein complexes (2–4). However, the precise role of the LIM domain is still unclear. Several distinct subgroups of the LIM domain–containing proteins are defined and some of them also possess a functionally divergent domain, including a DNA-binding homeodomain or a protein kinase domain (1, 2).

The LIM-only proteins (LMO) are one of the families of the LIM domain–containing proteins and possess only two tandem LIM domains. They consist of four members, including LMO1, LMO2, LMO3, and LMO4 (2, 4). *LMO1* and *LMO2* have been identified as the genes that are activated in human acute T-cell leukemia (T-cell ALL) by tumor-specific chromosomal translocations (4). Transgenic mice overexpressing LMO1 or LMO2 developed immature and aggressive T-cell leukemia, suggesting that these proteins act as T-cell oncoproteins (5–7). On the other hand, LMO4 has been identified as a nuclear protein that interacts with the adaptor protein Ldb1 (8). It has been shown recently that LMO4 is highly expressed in primary human breast cancers, and overexpression of LMO4 inhibits differentiation of mammary epithelial cells, suggesting that deregulated expression of LMO4 contributes to the breast carcinogenesis (9). LMO4 has also been reported to be associated with BRCA1 to repress its transcriptional activity (10). Thus, LMO1, LMO2, and LMO4 have been implicated in tumorigenesis. However, to date, little is known about the oncogenic function of LMO3, which has been discovered based on sequence homology with LMO1 (11).

The nuclear LMO proteins, which lack intrinsic DNA-binding activity, have been considered to be involved in transcriptional regulation (2), raising a possibility that they alter the transcription of target genes by forming a complex with other transcription factors with DNA-binding activity. Indeed, in T-cell acute lymphoblastic leukemia in children, a basic helix-loop-helix transcription factor, TAL1, is physically associated with LMO1 or LMO2 and enhances their oncogenic activities (12, 13). Interestingly, the neuronal-specific basic helix-loop-helix transcription factors, HEN1 and HEN2, were identified based on cross-hybridization with TAL1 (14, 15). Their expression was restricted to the developing nervous system and a human neuroblastoma cell line. However, the role of HEN1 and HEN2 in tumorigenesis has long been elusive.

Neuroblastoma is one of the most common childhood cancers and is originated from sympathoadrenal lineage of the neural crest (16). It is clinically and cytogenetically divided into two major subgroups with favorable and unfavorable prognosis (17). The recent molecular and cellular analyses have revealed that amplification of *MYCN* and *DDX1* as well as loss of heterozygosity at the region of chromosome 1p36 are strongly associated with a poor outcome, whereas high levels of expression of the neurotrophin receptors *TrkA*, *CD44*, and *Fyn*, are well correlated with favorable prognosis (16–23). However, we still do not know many other genes that play important roles in the genesis and progression of neuroblastoma. To identify the other genes closely involved in neuroblastoma, we have constructed several cDNA libraries from different subsets of neuroblastoma and randomly cloned 4,200 genes (24). Screening of the genes differentially expressed between favorable and unfavorable subsets of the tumor has identified *Nbla3267* as one of the genes expressed at higher levels in unfavorable than favorable neuroblastomas (25).

In the present study, we found that *Nbla3267* encoded the human LMO, LMO3, and that high expression of *LMO3* as well as *HEN2* was strongly associated with a poor prognosis of neuroblastoma. Furthermore, LMO3 interacted with HEN2 in mammalian

Requests for reprints: Akira Nakagawara, Division of Biochemistry, Chiba Cancer Center Research Institute, 666-2 Nitona, Chuoh-ku, Chiba 260-8717, Japan. Phone: 81-43-264-5431; Fax: 81-43-265-4459; E-mail: akiranak@chiba-cc.jp.

cell nucleus, and enforced expression of LMO3 in human neuroblastoma-derived cell line SH-SY5Y markedly enhanced tumor growth in nude mice, supporting the oncogenic role of LMO3 in neuroblastoma.

Materials and Methods

Patient population. The RNA samples obtained from 87 patients with neuroblastoma were subjected to semiquantitative and quantitative real-time reverse transcription-PCR (RT-PCR) analyses. All patients were diagnosed clinically as well as pathologically and tested for DNA ploidy, MYCN amplification, and TrkA expression. Tumors were staged according to the International Neuroblastoma Staging System criteria (26). Thirty-four patients were stage I, 14 were stage II, 8 were stage III, 26 were stage IV, and 5 were stage IVS. Stages I, II, and IVS were considered as favorable and stages III and IV as unfavorable. The patients were treated following the protocols proposed by the Japanese Infantile Neuroblastoma Cooperative Study (27) and the Study Group of Japan for Treatment of Advanced Neuroblastoma (28). The clinical follow-up ranged from 4 to 58 months, with a median of 36 months. We have a precise list of patient characteristics, including age, stage, and clinical follow-up time, and this list will be provided upon request.

Cloning of human *LMO3*, *HEN1*, and *HEN2*. To obtain a complete human *LMO3* cDNA, a cDNA library derived from human fetal brain (Stratagene, La Jolla, CA) was screened with a ^{32}P-labeled *Nbla3267* cDNA. Plaques showing positive signals were picked up and rescreened twice. To construct the expression plasmid for hemagglutinin (HA)–tagged LMO3-A, the cDNA fragment encoding the entire LMO3-A protein was amplified by PCR from the phage clone as a template using the primers designed to add a synthetic linker encoding the HA epitope on the NH_2-terminal side of LMO3-A (forward 5′-GGTACCATGGCTTACCCATACGATGTTCCAGATTACGCTAGCCTCTCAGTCCAGCCAGACAC-3′ and reverse 5′-TCAGATATCATTAGATCAGCGAACCTGGG-3′). The PCR product was digested with *Kpn*I and *Eco*RV and subcloned into the identical restriction sites of pcDNA3 expression plasmid to give pcDNA3-HA-LMO3-A. cDNA encoding human HEN1 (amino acid residues 1-133) or HEN2 (amino acid residues 1-135) was generated by reverse transcribing total RNA isolated from neuroblastoma cell line, IMR32, using a forward primer (5′-AAGGAATTCATGCTCAACTCAGACACCATG-3′) and a reverse primer (5′-ATAAGAATGCGGCCGCTCAGACGT-3′) for HEN1 and a forward primer (5′-AAGGAATTCATGCTGAGTCCGGACCAAGCA-3′) and a reverse primer (5′-ATAAGAATGCGGCCGCCTACACGTCCAGGACGTGGTT-3′) for HEN2. The amplified PCR products were digested with *Eco*RI and *Not*I and subcloned into the identical restriction sites of pcDNA3-FLAG expression plasmid to give pcDNA-FLAG-HEN1 and pcDNA3-FLAG-HEN2.

Generation of a polyclonal anti-LMO3 antibody. The polyclonal anti-LMO3 and anti-HEN2 antibodies were raised against a peptide "Cys" plus containing the amino acid sequence between positions 127 and 145 of LMO3 and the amino acid sequence between positions 1 and 19 of HEN2, respectively. The peptides and the polyclonal antibodies were produced by Biologica Co. (Nagoya, Japan).

Cell culture and transfection. Human neuroblastoma (SK-N-AS, SH-SY5Y, NB69, OAN, SK-N-BE, NGP, NLF, IMR32, NB1, and KP-N-NS), ALL (RPMI, KOPT, HSB, and MOLT), osteosarcoma (OST, SAOS-2, and U2OS), rhabdomyosarcoma (RMS-MK), colon cancer (COLO-320), breast cancer (MCF-7 and MDA-MB-453), melanoma (G361, G32TG, and A875), thyroid cancer (TTC11), small cell lung carcinoma (H1299), and cervical cancer (HeLa) cell lines and COS7 cells were maintained in RPMI 1640 or DMEM supplemented with 10% heat-inactivated fetal bovine serum (FBS), 100 IU/mL penicillin, and 100 μg/mL streptomycin at 37°C in an atmosphere of 5% CO_2 in the air. For transient transfection, COS7 cells were transfected with the indicated expression plasmids using FuGene 6 transfection reagent as recommended by the manufacturer (Roche Molecular Biochemicals, Mannheim, Germany). Stable transfections of SH-SY5Y cells were done with the empty plasmid (pcDNA3, Invitrogen, Carlsbad, CA) or with the expression plasmid for FLAG-tagged LMO3-A using Lipofect-AMINE Plus transfection reagent according to the manufacturer's instructions (Invitrogen). The transfected cells were cultured in the presence of G418 at a final concentration of 400 μg/mL (Sigma Chemical Co., St. Louis, MO). Thereafter, the selection medium was replaced every 3 days. Three weeks after the selection in G418, drug-resistant clones were isolated and allowed to proliferate in medium containing G418.

Reverse transcription-PCR analysis. Total RNA was prepared from cultured cells and human tissues by using Trizol reagent (Life Technologies, Grand Island, NY) or the RNeasy Mini kit (Qiagen, Valencia, CA). Reverse transcription was carried out using random primers and SuperScript II (Invitrogen). Following the reverse transcription, the resultant cDNA was subjected to PCR-based amplification. Oligonucleotides used to amplify *LMO3-A*, *LMO3-B*, *LMO1*, *LMO2*, *LMO4*, *Ldb1*, *Ldb2*, *TAL1*, *HEN1*, *HEN2*, and glyceraldehyde-3-phosphate dehydrogenase (*GAPDH*) mRNAs were as follows: *LMO3-A*: forward 5′-ACTGTGCTTACTGAACGGCCTC-3′ and reverse 5′-CCGGTCCTTGATCTTTCGGTTG-3′; *LMO3-B*: forward 5′-TGCAACTCAGACACGCCTAAG-3′ and reverse 5′-CCGGTCCTTGATCTTTCGGTTG-3′; *LMO1*: forward 5′-GCTCCACCCTCTACACCAAG-3′ and reverse 5′-CTGCCCTTCCTCATAGTCCA-3′; *LMO2*: forward 5′-AATGCGGGTGAAAGACAAAG-3′ and reverse 5′-CCCCAAAGTGCCTAAGAGTG-3′; *LMO4*: forward 5′-GCAAGGCAATGTGTATCATCT-3′ and reverse 5′-GCATTCTGCATTACTCTGACC-3′; *Ldb1*: forward 5′-CCAGGGAGCAGAAGACAGAA-3′ and reverse 5′-AGAGGCCCAGGTTCCAAG-3′; *Ldb2*: forward 5′-TAGCCCAAGTGCTGAAACAA-3′ and reverse 5′-TAAACTGCCCACAAAACCAA-3′; *TAL1*: forward 5′-GTTCTTAGGCTGCTGGGATG-3′ and reverse 5′-GATTTGGGACTGAGGGAAGA-3′; *HEN1*: forward 5′-AGAGACTGAGTCGGGCTTCA-3′ and reverse 5′-CAGGCGCAGAATCTCAATCT-3′; *HEN2*: forward 5′-CCCCAAGGGTTGTGGTTTTA-3′ and reverse 5′-TCTGAACTTCTGCCCTCATTCTTT-3′; and *GAPDH*: forward 5′-ACCTGACCTGCCGTCTAGAA-3′ and reverse 5′-TCCACCACCCTGTTGCTGTA-3′. Amplified products were electrophoretically separated on agarose gels and visualized by ethidium bromide staining. The gels were photographed under UV illumination.

Northern analysis. A human MTN blot (Clontech, Palo Alto, CA), a nylon membrane on which poly(A)$^+$ RNAs extracted from various human normal tissues were blotted, was used for analysis of the distribution of *LMO3* expression in human normal tissues. ^{32}P-labeled probe was prepared by random priming of the 2.5-kb restriction fragment of *LMO3* cDNA. The membrane was hybridized overnight at 65C in a solution containing 7.5% dextran sulfate, 1 mol/L NaCl, 1% *N*-lauroyl sarcosine, 100 μg/mL heat-denatured salmon sperm DNA, and the radiolabeled probe. The membrane was washed twice in 0.5 × SSC/0.1% *N*-lauroyl sarcosine at 50°C. Specific signals were obtained by autoradiography.

Section *in situ* hybridization. Section *in situ* hybridization was done as described previously (29). A riboprobe was synthesized with digoxygenin-UTP and T3 or T7 polymerase (Roche Molecular Biochemicals). The alkaline phosphatase reaction was done with nitroblue tetrazolium/5-bromo-4-chloro-3-indolyl phosphate (Roche Molecular Biochemicals). The riboprobe used for the section *in situ* hybridization were transcripts of the human cDNA fragments of the *LMO3* gene.

Immunohistochemistry. Neuroblastoma tissues were stained with immunoperoxidase method using anti-HEN2 antibody. They included unfavorable neuroblastomas with *MYCN* gene amplification and favorable neuroblastomas with a single copy of *MYCN* gene. Neuroblastoma specimens were fixed in 10% buffered formalin and embedded in paraffin, and 3 μm sections were applied to the immunostaining. Before incubation with anti-HEN2 antibody, the sections were treated with 0.05% Pronase in 0.05 mol/L Tris-HCl (pH 7.6) for 5 minutes. The sections were incubated with anti-HEN2 antibody, which was diluted to 1:200 at 4°C overnight. The biotin-streptavidin method (Nichirei, Tokyo, Japan) was done, and the sections were visualized with diaminobenzidine solution. The nuclei were counterstained with hematoxylin.

Immunofluorescent staining. COS7 cells were doubly transfected with the expression plasmids for HA-LMO3-A and FLAG-HEN2. Forty-eight hours after transfection, cells were fixed for 30 minutes with 3.7% formaldehyde in PBS and permeabilized with 0.2% Triton X-100 for 5 minutes, and nonspecific epitopes were blocked for 1 hour in PBS containing 3% bovine serum albumin. The cells were then incubated with a polyclonal anti-HA antibody (1:200 dilution, Medical and Biological Laboratories, Nagoya,

Japan) and a monoclonal anti-FLAG antibody (1:50, M2, Sigma Chemical). After three washes with PBS, cells were stained with a FITC- or a rhodamine-conjugated secondary antibody (1:200, Invitrogen). The coverslips were mounted onto glass slides, and the stained cells were viewed using a confocal laser scanning microscope (Olympus, Tokyo, Japan).

Western blot analysis and immunoprecipitation. After transfection, cells were rinsed twice with ice-cold PBS and then lysed immediately with SDS sample buffer. Equal amounts of proteins were separated under denaturing conditions by electrophoresis in 15% polyacrylamide gel containing SDS-PAGE and electrotransferred to polyvinylidene difluoride membrane (Immobilon-P, Millipore, Bedford, MA). After blocking in a solution containing 5% skim milk, the membrane was incubated with a monoclonal anti-FLAG, a polyclonal anti-HA, a polyclonal anti-LMO3, or a polyclonal anti-actin antibody (20-33, Sigma Chemical) and then incubated with a horseradish peroxidase–conjugated goat anti-mouse or anti-rabbit secondary antibody (Jackson ImmunoResearch Laboratories, West Grove, PA). Protein bands were visualized with an enhanced chemiluminescence (Amersham Pharmacia Biotech, Piscataway, NJ). For immunoprecipitation, transfected cells were lysed in EBC buffer [50 mmol/L Tris-HCl (pH 7.5), 120 mmol/L NaCl, 0.5% NP40, 1 mmol/L phenylmethylsulfonyl fluoride] containing protease inhibitor mixture (Sigma Chemical). The precleared soluble supernatants were mixed with a polyclonal anti-HA or a monoclonal anti-FLAG antibody and incubated for 2 hours at 4°C. Protein A-Sepharose beads were then added to the reaction mixtures and incubated for 1 hour at 4°C. The immune complexes were washed with the lysis buffer thrice at 4°C. The bound proteins were resuspended in SDS sample buffer, resolved by SDS-PAGE, and analyzed by Western blotting.

Cell proliferation and soft agar assay. Cells were seeded in triplicate in 24-well plates (5×10^3 per well) in culture medium containing 10% or 1% FBS. Cells were allowed to adhere to the bottom of the cell culture dish for 24 hours. At the indicated times, cells were trypsinized and cell counting was carried out using a Coulter Counter (Coulter Electronics Ltd., Hialeah, Finland). For soft agar assay, 2.5×10^3 cells of the stable transfectants or the parental SH-SY5Y cells were seeded in triplicate in 35-mm cell culture plates containing 0.2% agar and RPMI 1640 supplemented with 10% FBS. After 21 days, colonies with diameters >300 μm were scored as positive.

Tumor formation in nude mice. For tumor formation, 6-week-old female athymic *nu/nu* mice (Charles River Laboratory, Sulzfeld, Germany) were injected into the femur with 5×10^6 parental SH-SY5Y cells or SH-SY5Y cells transfected with the empty plasmid or with the expression plasmid encoding LMO3-A suspended in 100 μL PBS. Tumor size and body weight were measured once weekly and mice were sacrificed 7 weeks after injection. For histologic examinations, tumor tissues were fixed in fresh 10% buffered formalin and embedded in paraffin. The handling of animals was in accordance with the guidelines of the Chiba Cancer Center Research Institute (Chiba, Japan).

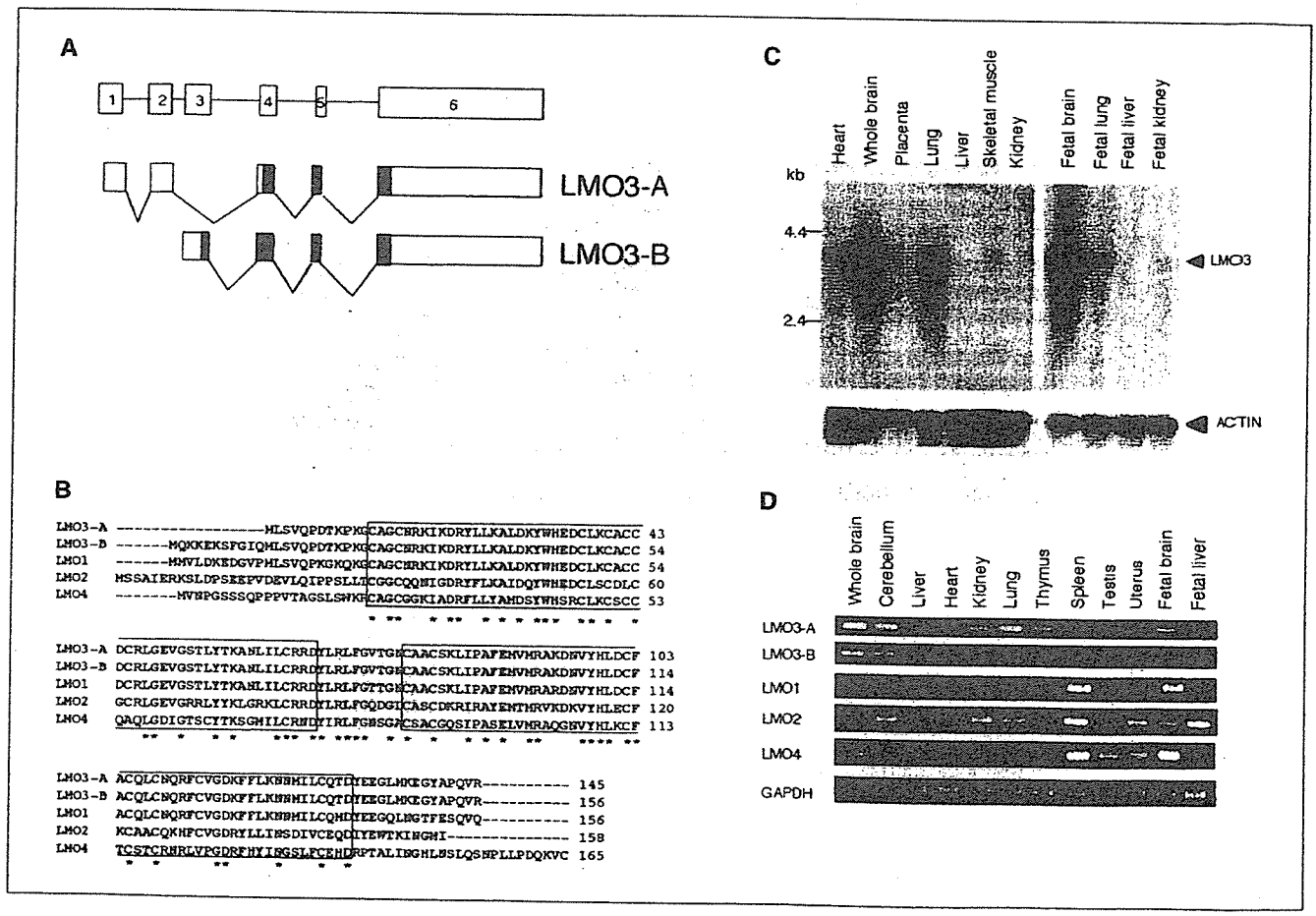

Figure 1. Identification of human LMO3-A and LMO3-B and their relation to the other LMO family members. *A*, schematic representation of the exons of human *LMO3* gene. *Solid* and *open boxes*, coding and untranslated regions, respectively. *B*, deduced amino acid sequences of human LMO3-A and LMO3-B and their alignments with those of human LMO1, LMO2, and LMO4. *Asterisks*, identical amino acid residues. Two LIM domains are *boxed*. *C*, tissue-specific expression of *LMO3*. Human multiple tissue Northern blots containing poly(A)$^+$ RNA were hybridized with a radiolabeled human *LMO3* cDNA (*top*) or with a radioactive probe derived from human *β-actin* cDNA (*bottom*). β-actin was used as a control for equal loading. The 2-kb band was hybridized ubiquitously, and an additional 4.8-kb band was hybridized in heart and skeletal muscle with the β-actin probe. *D*, coordinated expression of *LMO3-A* and *LMO3-B* in various human tissues. Total RNA isolated from the indicated human tissues was subjected to RT-PCR analysis to examine the expression levels of *LMO3-A*, *LMO3-B*, *LMO1*, *LMO2*, and *LMO4*. *GAPDH* expression is shown as an internal control.

Quantitative real-time PCR. Total RNA prepared from primary neuroblastomas was reverse transcribed into cDNA (SuperScript II kit) and subjected to the real-time PCR. The expression level of *GAPDH* was measured in all samples to normalize *LMO3* and *HEN2* expression according to the manufacturer's instructions (Applied Biosystems, Foster City, CA). Oligonucleotide primers and TaqMan probes, which were labeled at the 5′ end with the reporter dye 6-carboxyfluorescein (FAM) and at the 3′ end with the quencher dye 6-carboxytetramethylrhodamine (TAMRA), were as follows: *LMO3*: forward 5′-TCTGAGGCTCTT-TGGTGTAACG-3′, reverse 5′-CCAGGTGGTAAACATTGTCCTTG-3′, and probe 5′-FAM-AAACTGCGCTGCCTGTAGTAAGCTCATCC-TAMRA-3′ and *HEN2*: forward 5′-CCCCAAGGGTTGTGGTTTTA-3′, reverse 5′-TCTGAACTTCTGCCCTCATTCTTT-3′, and probe 5′-FAM-TTGAGTTCTCC-TACATTCATCCGCCACAA-TAMRA-3′. Amplification and detection were done using the ABI Prism 7700 Sequence Detection System (Applied Biosystems).

Statistical analysis. Student's *t* tests were used to explore possible associations between *LMO3* expression and other factors. Because the values of the *LMO3* expression were skewed, a log transformation was used to achieve the normality in the analyses using *t* test and Cox regression. The distinction between high and low levels of *LMO3* expression was based on the median value (low, *LMO3* < 0.2493 e.u.; high, *LMO3* > 0.2493 e.u.) regardless of tumor stage, *MYCN* copy number, or survival. The distinction between high and low levels of *HEN2* expression was based on the distribution of the values (low, undetectable; high, detectable). χ^2 tests were used to examine possible associations between *HEN2* expression and other factors, such as tumor stage. Kaplan-Meier survival curves were calculated, and survival distributions were compared using the log-rank test. Cox regression models were used to explore associations among *LMO3* expression, *HEN2* expression, age, *MYCN* amplification, mass screening, origin, and survival. Statistical significance was declared if $P < 0.05$. The statistical analysis was done using Stata Statistical Software Release 7.0 (Stata Corp., College Station, TX, 2001).

Results

Identification of the human *LMO3* gene. To identify the genes specifically involved in the genesis and progression of neuroblastoma, we have previously constructed cDNA libraries from the primary neuroblastomas and screened for the differentially expressed genes between the tumors with good and poor clinical outcome (25). One of the cDNA clones, *Nbla3267*, significantly overexpressed in the poor prognostic neuroblastomas contained a partial nucleotide sequence encoding a LMO family protein, LMO3. To obtain the missing 5′ part of the *LMO3* cDNA, we screened a cDNA library derived from human fetal brain. From $\sim 6 \times 10^5$ recombinant phage clones, 10 independent phage clones were isolated. Sequence analysis

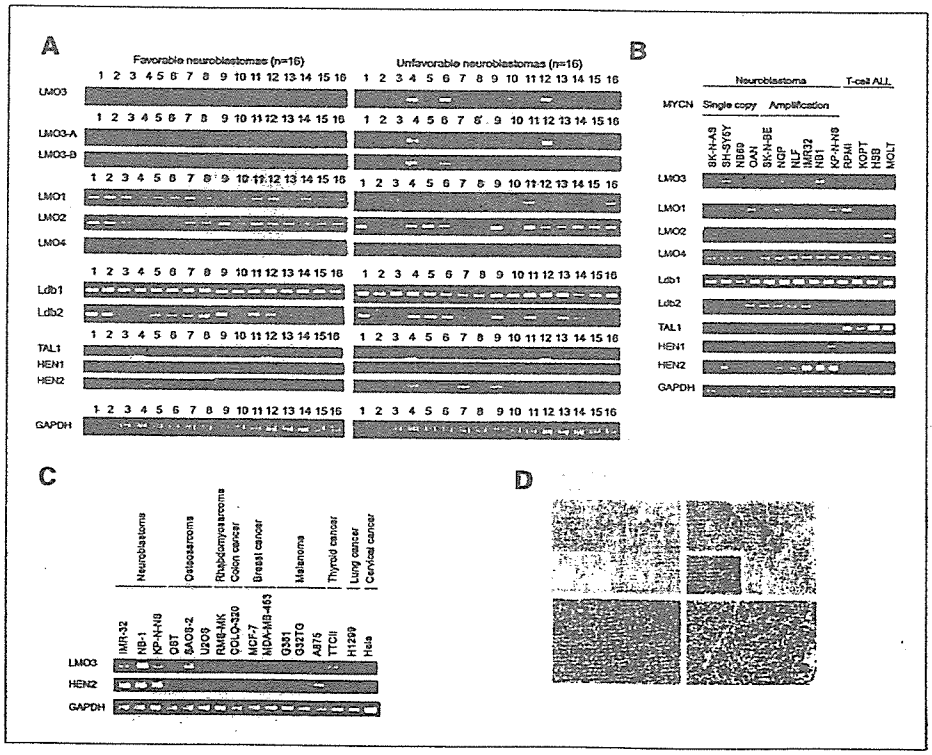

Figure 2. Increased expression of *LMO3* and *HEN2* in unfavorable neuroblastomas and neuroblastoma-derived cell lines. *A*, expression of *LMO3* and *LMO*-related genes in primary neuroblastomas with favorable (stage I, a single copy of *MYCN* and high expression of *TrkA*) and unfavorable (stages III and IV, *MYCN* amplification and decreased expression of *TrkA*) characteristics. Total RNA was isolated from the indicated neuroblastoma tissues, reverse transcribed, and amplified by PCR to examine the expression levels of *LMO3*, *LMO3-A*, *LMO3-B*, *LMO1*, *LMO2*, *LMO4*, *Ldb1*, *Ldb2*, *TAL1*, *HEN1*, and *HEN2*. Expression of *GAPDH* serves as an internal control. PCR products were visualized by ethidium bromide staining. *B*, expression of *LMO3* and *LMO*-related genes in neuroblastoma cell lines without *MYCN* amplification (SK-N-AS, SH-SY5Y, NB69, and OAN), neuroblastoma cell lines with *MYCN* amplification (SK-N-BE, NGP, NLF, IMR32, NB1, and KP-N-NS), and ALL cell lines (RPMI, KOPT, HSB, and MOLT). Total RNA prepared from the indicated cultured cells was subjected to RT-PCR analysis. Expression of *GAPDH* serves as an internal control. *C*, expression of *LMO3* and *HEN2* in various tumor-derived cell lines. Total RNA prepared from the indicated culture cells was subjected to RT-PCR analysis as described above. *D*, section *in situ* hybridization of neuroblastoma with the *LMO3* probe. Serial sections of the favorable neuroblastoma tissue (*top left* and *inset*) or the unfavorable one with *MYCN* amplification (*top right* and *inset*) were prepared, and expression of the *LMO3* gene was examined by section *in situ* hybridization. The *LMO3* transcripts are positive in unfavorable neuroblastoma. Immunohistochemical staining of HEN2 in primary neuroblastoma tissues. HEN2 is strongly positive in the nucleus of most tumor cells with *MYCN* amplification (*bottom right*), whereas it is negative in the favorable neuroblastoma tissue (*bottom left*).

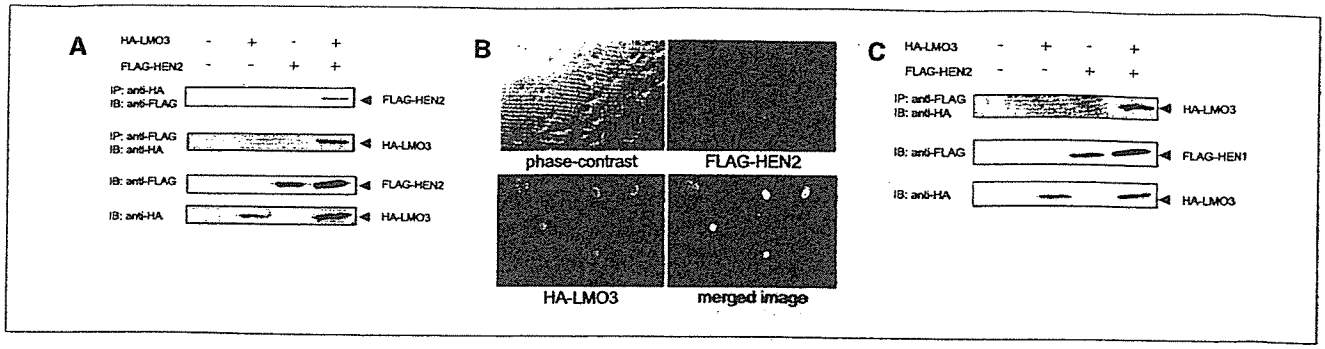

Figure 3. LMO3 interacts with HEN2 in mammalian cells. *A*, coimmunoprecipitation analysis. COS7 cells were transfected with the indicated expression plasmids. Forty-eight hours after transfection, whole cell lysates were prepared and subjected to the immunoprecipitation/Western analysis (*top* and *top middle*). Whole cell lysates were monitored on immunoblot for the expression of FLAG-HEN2 (*bottom middle*) and HA-LMO3-A (*bottom*). *B*, nuclear colocalization of LMO3 and HEN2 in cultured cells. COS7 cells were cotransfected with the expression plasmids for HA-LMO3-A and FLAG-HEN2. Forty-eight hours after transfection, cells were fixed and incubated with the polyclonal anti-HA and monoclonal anti-FLAG antibodies. Cells were then processed for double immunofluorescence using the FITC-conjugated anti-rabbit IgG (*green*) and with the rhodamine-conjugated anti-mouse IgG (*red*). The merged images (*yellow*) suggest the nuclear colocalization of LMO3 and HEN2. The phase-contrast images are also shown. *C*, coimmunoprecipitation of FLAG-HEN1 and HA-LMO3. Whole cell lysates prepared from COS7 cells transfected with the indicated combinations of the expression plasmids were immunoprecipitated with the anti-FLAG antibody followed by immunoblotting with the anti-HA antibody (*top*). Levels of FLAG-HEN1 and HA-LMO3 were also examined by immunoblotting with the anti-FLAG antibody (*middle*) and with the anti-HA antibody (*bottom*), respectively.

revealed that they were divided into two types, designated LMO3-A (145 amino acids) and LMO3-B (156 amino acids), with the different translation initiation sites. The NH_2-terminal region of LMO3-A was identical to that of the previously reported LMO3 protein (11). As shown in Fig. 1*A*, the putative translation initiation sites of LMO3-A and LMO3-B were located within exons 4 and 3, respectively. Because *LMO3* is a single gene, it is likely that LMO3-A and LMO3-B arise from differential splicing

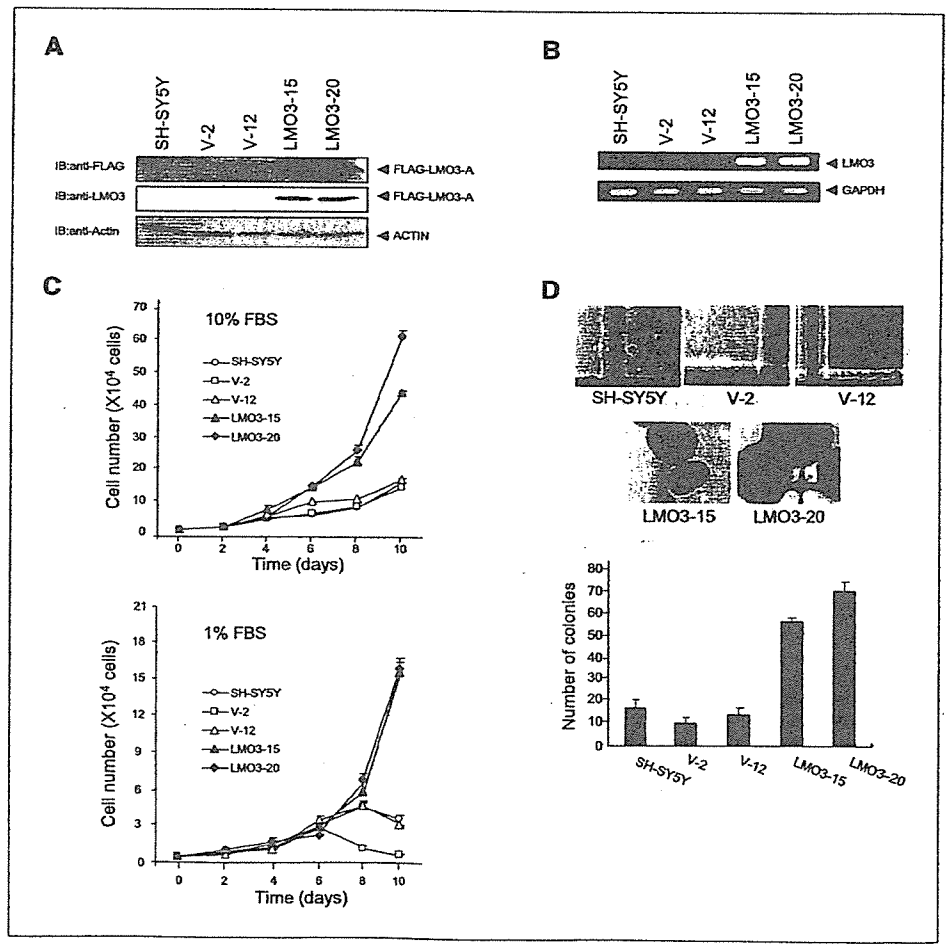

Figure 4. Growth-promoting activity of LMO3 in SH-SY5Y cells. *A*, stable SH-SY5Y transfectants expressing exogenous FLAG-LMO3-A. SH-SY5Y cells were stably transfected with the empty plasmid or with the expression plasmid for FLAG-LMO3-A and maintained in the presence of G418 (at a final concentration of 400 μg/mL) for 3 weeks. Whole cell lysates prepared from the indicated drug-resistant cell clones in addition to the parental SH-SY5Y cells were subjected to Western blot analysis using the anti-FLAG (*top*), anti-LMO3 (*middle*), or anti-actin (*bottom*) antibody. *B*, RT-PCR analysis of LMO3 in the indicated stable transfectants along with the parental SH-SY5Y cells. Expression of GAPDH serves as an internal control. *C*, effects of LMO3 overexpression on cell growth in SH-SY5Y cells. SH-SY5Y cells and the indicated transfectants were grown in the culture medium containing 10% (*top*) or 1% (*bottom*) FBS. Cells were harvested at 48-hour time intervals and number of cells was counted in triplicate. *Points*, means from three independent experiments; *bars*, SE. *D*, anchorage-independent growth of LMO3-overexpressing transfectants. The parental SH-SY5Y cells and the indicated transfectants (2.5×10^3 cells per dish) were grown in soft agar medium. After 3 weeks of culture, cells were examined by phase-contrast microscopy (*top*), and the numbers of colonies with a diameter of >300 μm were counted (*bottom*). *Columns*, means from three independent experiments; *bars*, SE.

or alternative promoter usage. Amino acid sequence alignment of LMO3 with the other LMO family proteins (LMO1, LMO2, and LMO4) showed a significant homology among them (Fig. 1*B*). LIM domains of LMO3 presented 98%, 60%, and 55% amino acid homology with those of LMO1, LMO2, and LMO4, respectively.

To determine the expression pattern of human *LMO3* mRNA, we did Northern blot analysis on a human multiple tissues blot using -actin as a control. As shown in Fig. 1*C*, *LMO3* mRNA (~4 kb) was abundantly expressed in brain and at relatively low levels in the heart and lung but not in the other tissues examined. Similar to the adult tissues, *LMO3* mRNA was expressed predominantly in fetal brain, with a lower level in fetal lung. We then compared the tissue distribution of *LMO3-A* expression with those of *LMO3-B* and the other *LMO* family gene expression in various human adult and fetal tissues by RT-PCR (Fig. 1*D*). The expression pattern of *LMO3-A* was similar to that of *LMO3-B*, with relatively higher levels in brain, cerebellum, and fetal brain. In contrast, *LMO2* and *LMO4* were expressed ubiquitously in human tissues, and *LMO1* was expressed at higher levels in spleen and fetal brain.

Expression of *LMO3* and *HEN2* in aggressive neuroblastomas. As described previously, LMO family protein interacts with the nuclear LIM domain–binding protein 1 and 2 (Ldb1 and Ldb2), which act as adaptors for several LIM domain–containing proteins (30–32), and also binds to the basic helix-loop-helix transcription factor, TAL1, to regulate its transcriptional activity (12, 33, 34). Of interest, HEN1 and HEN2 were previously identified based on their homology with TAL1, and it was shown that LMO3 was associated with HEN1 (35). Furthermore, TAL1 was coexpressed with LMO1 or LMO2 in T-cell ALL (36), and double transgenic mice overexpressing TAL1 and LMO1 or LMO2 developed leukemia (37). As shown in Fig. 2*A*, *LMO3* (A and B) and *HEN2* were expressed at higher levels in unfavorable neuroblastomas compared with favorable tumors, whereas the levels of *LMO1* expression were predominantly high in the favorable tumors. No significant changes in the expression levels of *LMO2*, *Ldb1*, and *Ldb2* were detected between unfavorable and favorable neuroblastomas. *LMO4*, *TAL1*, and *HEN1* showed extremely low levels of expression in both types of neuroblastoma. We then studied the expression of these genes in 10 neuroblastoma and 4 T-cell ALL cell lines to examine the presence or absence of the lineage specificity, neuronal or hematopoietic. Consistent with the previous reports (36), *LMO2* and *TAL1* were coexpressed in T-cell ALL-derived cell lines (RPMI, KOPT, HSB, and MOLT; Fig. 2*B*). However, of interest, *LMO3* and *Ldb2* were expressed predominantly in neuroblastoma cell lines compared with the leukemia-derived lines. In addition, *HEN2* tended to be less highly expressed in leukemia cells compared with neuroblastoma cells. *HEN1* expression was also restricted to neuroblastoma but limited to only a few cell lines. On the other hand, there was no difference in the expression of *LMO4* and *Ldb1* between neuroblastoma-derived and T-cell ALL-derived cell lines. Interestingly, coexpression of *LMO3* and *HEN2* was observed in the majority of neuroblastoma cell lines but not in the other tumor-derived cell lines with different origin (Fig. 2*C*). These results revealed that only *LMO3* and *HEN2* were expressed at high levels in aggressive neuroblastomas in a neuronal-specific pattern.

Figure 2*D* shows the results of *in situ* hybridization for *LMO3* in primary neuroblastomas. *LMO3* mRNA was expressed in a stage IV neuroblastoma with *MYCN* amplification, whereas it was negative in a stage I tumor with a single copy of *MYCN* and high expression of *TrkA*. Unfortunately, our antibody raised against human LMO3 protein did not work for the immunohistochemical analysis. The immunostaining of HEN2 was also strongly positive in the nuclei of most tumor cells in *MYCN*-amplified neuroblastoma, albeit it was negative in favorable subset of the tumor (Fig. 2*D*).

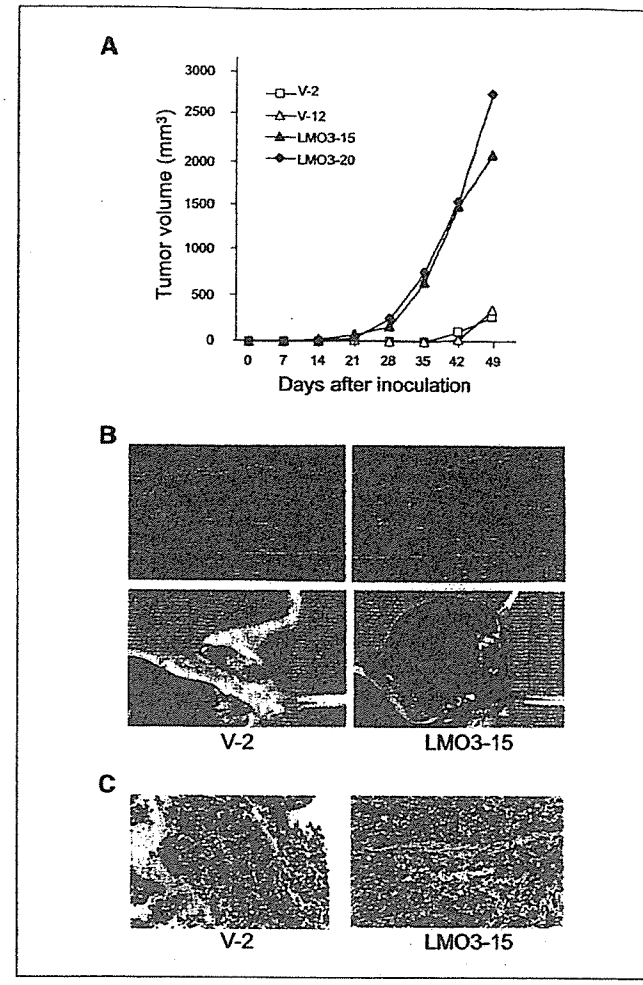

Figure 5. Tumor growth in nude mice. *A*, nude mice were injected s.c. with 5×10^6 of SH-SY5Y cells or the indicated stable transfectants and tumor volumes were estimated weekly. *Points*, mean of 8 to 11 independent tumors. *B*, photographs of the tumors 49 days after s.c. injection of V-2 (*left*) and LMO3-15 cells (*right*) into nude mice. *C*, paraffin sections of the tumors arising from V-2 (*left*) and LMO3-15 cells (*right*) were stained with H&E.

LMO3 physically interacts with HEN2. Because LMO3 and HEN2 were coexpressed in the majority of unfavorable neuroblastomas as well as neuroblastoma cell lines, we examined whether LMO3 could interact with HEN2 in mammalian cells. Whole cell lysates prepared from COS7 cells transfected with the expression plasmids for HA-tagged LMO3 and FLAG-tagged HEN2 were immunoprecipitated with the anti-HA or with the anti-FLAG antibody followed by immunoblotting with the anti-FLAG or with the anti-HA antibody, respectively. As shown in Fig. 3*A*, FLAG-HEN2 was coimmunoprecipitated with HA-LMO3. We then examined the subcellular distribution of LMO3 and

HEN2. COS7 cells were cotransfected with the expression plasmids for HA-LMO3 and FLAG-HEN2 and double stained with anti-HA and anti-FLAG antibodies. As shown in Fig. 3*B*, LMO3 as well as HEN2 appear exclusively nuclear. On closer inspection by merging two images, these two proteins colocalized in the nucleus. Consistent with the previous reports (35), HA-LMO3 was coimmunoprecipitated with FLAG-HEN1 under our experimental conditions (Fig. 3*C*).

Overexpression of LMO3 accelerates growth of SH-SY5Y neuroblastoma cells. We addressed the question whether LMO3 could induce cell growth of neuroblastoma. To this end, we transfected the expression plasmid for FLAG-LMO3-A or the empty plasmid into SH-SY5Y neuroblastoma cells and established two stable transfectants overexpressing FLAG-LMO3-A (named as LMO3-15 and LMO3-20). As shown in Fig. 4*A*, the expression levels of FLAG-LMO3-A were higher in LMO3-15 and LMO3-20 cells than in the parental SH-SY5Y and the control transfectants (V-2 and V-12). LMO3-15 expressed FLAG-LMO3-A at the level comparable with that in LMO3-20. Similar results were also obtained by RT-PCR analysis (Fig. 4*B*). No obvious morphologic changes could be observed in LMO3-15 and LMO3-20 cells (data not shown). As shown in Fig. 4*C*, LMO3-15 and LMO3-20 cells proliferated at a much faster rate than the control transfectants and SH-SY5Y cells in culture medium containing 10% serum. More importantly, LMO3-15 and LMO3-20 cells continued to grow exponentially even in the low serum culture medium, whereas the growth of the vector-transfected cells as well as SH-SY5Y cells was significantly suppressed under this condition.

To examine whether the LMO3-A-overexpressing cells have an ability to grow in soft agar medium, each transfectants were cultured in soft agar medium for 3 weeks. The numbers of colonies with diameters >300 μm formed by each transfectants in soft agar were scored. LMO3-15 and LMO3-20 cells formed large distinct colonies and showed a statistically significant increase in the number of colonies compared with the vector-transfected cells and SH-SY5Y cells (Fig. 4*D*). These results strongly suggest that overexpression of LMO3 is sufficient to induce malignant transformation in neuroblastoma cells. We also tried to obtain the cells stably transfected with HEN2 but never been successful with unknown reason.

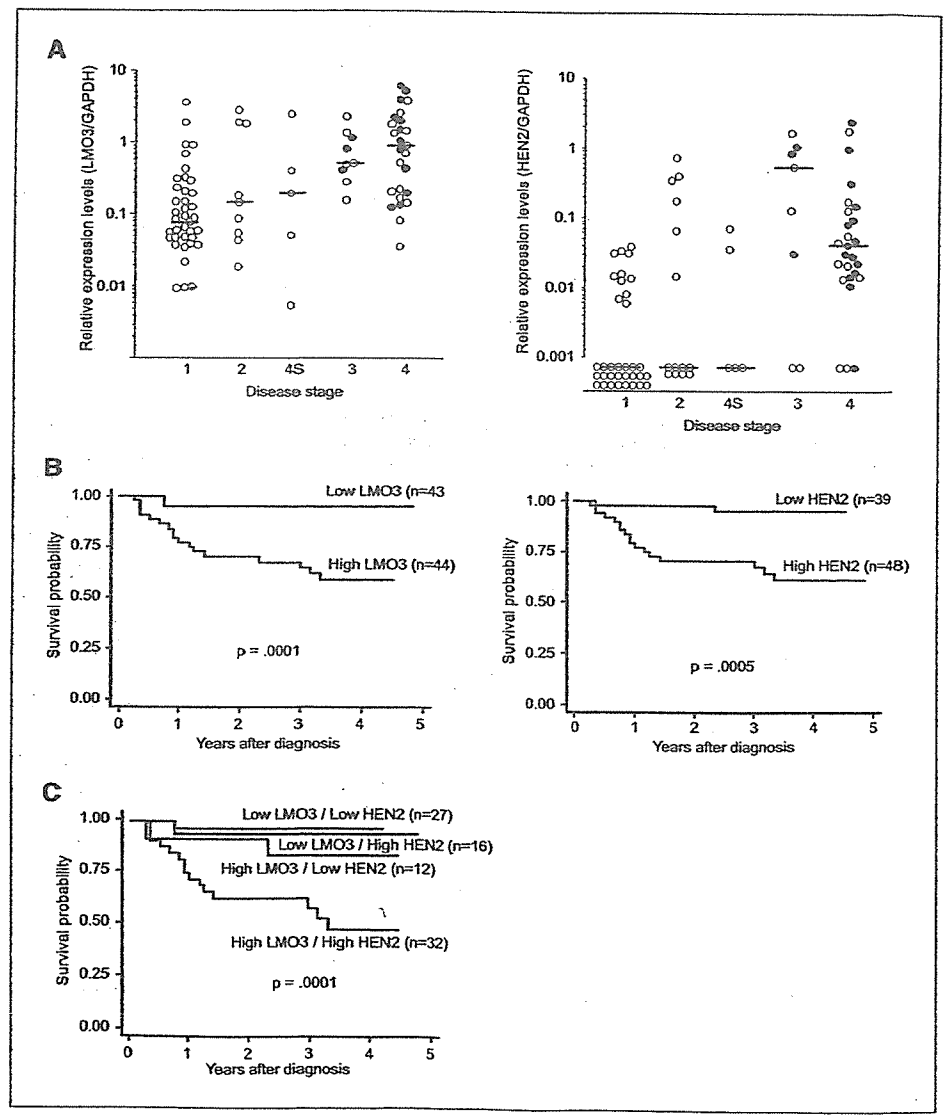

Figure 6. Expression of *LMO3* and *HEN2* mRNA in 87 primary neuroblastomas. *A*, expression levels of *LMO3* (*left*) and *HEN2* (*right*) transcripts in 87 primary neuroblastoma samples categorized by the patient's clinical stage were examined by a quantitative real-time RT-PCR. Relative expression levels of *LMO3* or *HEN2* mRNA were determined by calculating the ratio between *GAPDH* and *LMO3* or *HEN2*. *Bars*, median levels of *LMO3* or *HEN2* expression in each stage; *open* and *closed circles*, samples from patients who are alive and dead, respectively. *B* and *C*, Kaplan-Meier survival curves of patients with neuroblastomas based on high or low expression of *LMO3*, *HEN2* (*B*), or *LMO3* and *HEN2* (*C*).

LMO3 induces marked tumor growth in nude mice. SH-SY5Y cells with a single copy of *MYCN* form tumors in nude mice, although the growth rate is slow compared with that of the other neuroblastoma cell lines with *MYCN* amplification (38). To examine whether overexpression of LMO3 in SH-SY5Y cells could affect the tumor growth *in vivo*, we injected the each transfectants into the left flank of athymic nude mice, and the tumor volumes were measured weekly. V-2 and V-12 cells slowly formed tumors with similar kinetics and of similar sizes 35 to 42 days after injection (Fig. 5*A*). In contrast, the tumors grew rapidly in nude mice implanted with LMO3-15 or LMO3-20 cells. The sizes of the excised tumors from the LMO3-15-implanted mice on day 49 were >10-fold larger than those of control mice (Fig. 5*B*) and showed histologically undifferentiated neuroblastoma with small round cell shapes and small amounts of stromal components (Fig. 5*C*).

Expression of *LMO3* and *HEN2* is associated with a poor outcome of neuroblastoma. To verify whether a significant relationship could be observed between the expression of *LMO3* and/or *HEN2* in primary neuroblastomas and the patients' survival, we quantitatively measured the expression levels of *LMO3* and *HEN2* mRNA in 87 primary tumors by using a quantitative real-time RT-PCR. The values of the levels of *LMO3* and *HEN2* expression were normalized to that of *GAPDH* expression [relative expression values (REV)]. The high level of *LMO3* expression was significantly associated with high expression of *HEN2* (Student's *t* tests, mean ± SE: 1.43 ± 0.27 REV, n = 48 versus 0.54 ± 0.17 REV, n = 39; P = 0.001), older age (≥1-year-old: 1.37 ± 0.29, n = 32 versus <1-year-old: 0.84 ± 0.21, n = 55; P = 0.008), advanced disease stages (stages III + IV: 1.83 ± 0.35, n = 34 versus stages I + II + IVS: 0.52 ± 0.14; P < 0.00005; Fig. 6*A*), low levels of *TrkA* expression (low TrkA: 1.63 ± 0.34, n = 37 versus high *TrkA*: 0.59 ± 0.15, n = 50; P = 0.0003), *MYCN* amplification (amplification: 1.91 ± 0.44, n = 27 versus single copy: 0.64 ± 0.13, n = 60; P = 0.0002), and sporadic cases of neuroblastoma (sporadic: 1.68 ± 0.32, n = 39 versus mass screening: 0.51 ± 0.14, n = 48; P < 0.00005). The high level of *HEN2* expression was also significantly correlated with high expression of *LMO3* (χ^2 tests: P = 0.001), older age (P < 0.0005), advanced stages (P < 0.0005; Fig. 6*B*), low *TrkA* expression (P < 0.0005), *MYCN* amplification (P < 0.0005), and sporadic cases of neuroblastoma (P < 0.0005). Thus, high expression of *LMO3* and *HEN2* was well associated with conventional markers indicating the poor prognosis of neuroblastoma.

Table 1. Simple Cox regression models using LMO3 expression and dichotomous factors of HEN2 expression, age, MYCN amplification, mass screening, and origin (n = 87)

Model	Factor	P	Hazard ratio (95% confidence interval)
A	LMO3 expression (high vs low)	<0.0005	1.80 (1.32-2.47)
B	HEN2 expression (high vs low)	0.004	8.69 (2.00-37.7)
C	Age (≥1 vs <1 y)	<0.0005	8.75 (2.87-26.7)
D	MYCN amplification (1 copy vs >1 copy)	<0.0005	0.049 (0.014-0.171)
E	Mass screening (+ vs −)	0.001	0.032 (0.004-0.237)
F	Origin (adrenal gland vs others)	0.20	2.06 (0.684-6.23)

NOTE: All variables with two categories, except *LMO3* expression (log). Hazard ratio shows the relative risk of death of first category relative to the second. Because all patients with advanced tumor stages and low expression of *TrkA* had died of the tumor, a Cox regression model with the tumor stage or *TrkA* expression was not fitted.

Table 2. Multiple Cox regression models using LMO3 expression and dichotomous factors of HEN2 expression, age, MYCN amplification, mass screening, and origin (n = 87)

Model	Factor	P	Hazard ratio (95% confidence interval)
A	LMO3 expression (high vs low)	0.005	1.61 (1.16-2.23)
	HEN2 expression (high vs low)	0.029	5.32 (1.19-23.9)
B	LMO3 expression (high vs low)	0.005	1.62 (1.15-2.28)
	Age (>1 vs <1 y)	0.002	5.79 (1.86-18.1)
C	LMO3 expression (high vs low)	0.066	1.36 (0.98-1.89)
	MYCN amplification (1 copy vs >1 copy)	<0.0005	0.075 (.02-.282)
D	LMO3 expression (high vs low)	0.044	1.42 (1.01-2.01)
	Mass screening (+ vs −)	0.005	0.051 (0.007-0.404)
E	LMO3 expression (high vs low)	<0.0005	1.78 (1.31-2.41)
	Origin (adrenal gland vs others)	0.21	2.02 (0.666-6.12)

NOTE: All variables with two categories, except *LMO3* expression (log). Hazard ratio shows the relative risk of death of first category relative to the second.

We next tested if expression levels of *LMO3* and *HEN2* could have prognostic significance in primary neuroblastomas. The results for log-rank tests showed that high expression of *LMO3* or *HEN2* was significantly associated with poor survival (P = 0.0002 and 0.0005, respectively; Fig. 6*C* and *D*). Remarkably, the combination of high expression of both *LMO3* and *HEN2* showed the significantly worse prognosis compared with the other combinations of *LMO3* and *HEN2* expression levels as shown in Fig. 6*E*. As expected, older patients and the patients with advanced tumors, low expression of *TrkA*, amplified *MYCN*, and the tumors found by mass screening were associated with short time to survival (P < 0.00005). However, the adrenal origin of the tumor was not associated with the outcome (P = 0.19; data not shown).

The univariate analysis suggested that *LMO3* expression (P < 0.0005), *HEN2* expression (P = 0.004), age (P < 0.0005), *MYCN* amplification (P < 0.0005), and mass screening (P = 0.001) were of prognostic importance, supporting the results of the log-rank test (Table 1). Furthermore, the multivariate analysis showed that

LMO3 expression was significantly associated with survival after controlling *HEN2* expression ($P = 0.005$), age ($P = 0.005$), mass screening ($P = 0.044$), and origin ($P < 0.0005$), suggesting that *LMO3* expression was an independent prognostic factor from the other factors (Table 2). *LMO3* expression was marginally associated with survival after controlling *MYCN* amplification ($P = 0.066$). On the other hand, because *HEN2* expression was highly associated with age, *MYCN* amplification, and mass screening, it was not significantly associated with survival after controlling age, *MYCN* amplification, and mass screening in the corresponding multiple Cox regression models (data not shown).

Discussion

In the present study, we have identified that both *LMO3* and *HEN2* are expressed at higher levels in aggressive neuroblastomas especially with *MYCN* amplification than those with favorable prognosis. Coexpression of *LMO3* and *HEN2* has been observed almost exclusively in neuroblastoma cell lines, not the other lines, suggesting that their expression and function are neuronal specific. Furthermore, LMO3 physically interacted with HEN2 in mammalian cells. The functional significance of LMO3 expression was shown by a stable transfection into SH-SY5Y neuroblastoma cells, colony formation in soft agar, and tumor growth in nude mice, all of which have suggested that LMO3, probably by interacting with endogenous HEN2, markedly promotes the tumor growth. Indeed, the tumors with high expression of both *LMO3* and *HEN2* have shown the worst prognosis in the analysis of 87 primary neuroblastomas. Thus, our results suggested that, in concert with HEN2, the neuronal specifically expressed LMO3 plays an important role in the tumorigenesis of neuroblastoma. Our observation is strikingly intriguing because that *LMO1* or *LMO2* is already known to be the oncogene in T-cell acute lymphoblastic leukemia and that *LMO4* has recently been implicated in the genesis of breast cancer (4, 9).

We have identified a *Nbla3267/LMO3* clone from the screening of differentially expressed genes between favorable and unfavorable subsets of neuroblastoma. *LMO3* was one of the genes expressed at higher levels in the latter than the former (24), like *MYCN* oncogene and *DDX1*, a DEAD box gene coamplified with *MYCN* in aggressive neuroblastomas. In the development of hematopoietic system, LMO1 and LMO2 form a transcriptional complex with Ldb1, a LIM domain–binding protein, and a basic helix-loop-helix protein TAL1, which was identified as an oncogene at the translocation breakpoint in T-cell ALL (4–7). From the analogy with the LMO1 or LMO2 transcriptional machinery in T-cell ALL, we searched for the similar complex in the neuronal system by using the different subsets of primary neuroblastoma and the cell lines in comparison with the T-cell ALL cell lines. As a result, the neuronal-specific pattern of expression was observed in *LMO3*, *Ldb2*, *HEN1*, and *HEN2*, among which *LMO3* and *HEN2* were significantly highly expressed in the unfavorable subset of neuroblastomas with *MYCN* amplification compared with the favorable subset. This result strongly suggested that *LMO3* may function in collaboration with *HEN2* in advanced stages of neuroblastoma. Indeed, both genes were coexpressed only in neuroblastoma derived-cell lines, not in other tumor-derived ones, suggesting that their expression is lineage specific. Furthermore, LMO3 and HEN2 physically interacted in mammalian cells, albeit with weak interaction between LMO3 and HEN1 (35). Thus, these results also suggest that LMO3 and HEN2 form a neuronal cassette mimicking the hematopoietic complex composed of LMO2 and TAL1 and regulate the growth of neuroblastoma.

The neuronal-specific basic helix-loop-helix transcription factors, HEN1 and HEN2, were originally identified from the cDNA library of a neuroblastoma cell line based on cross-hybridization with TAL1 (14, 15). Their expression was restricted to the developing nervous system and a neuroblastoma cell line. However, their function has long been unclear. Recently, Bao et al. have reported that HEN1 interacts with LMO proteins by yeast two-hybrid screen and that *Xenopus* HEN1, in concert with XLMO3, is a critical regulator of neurogenesis (35). This prompted us to test our hypothesis both *in vitro* and *in vivo*. As the results, we found that the SH-SY5Y neuroblastoma cells stably overexpressing LMO3, presumably by acting with endogenous HEN2, gained rapid cell growth in the culture medium with 10% or 1% serum, in the soft agar medium, and in nude mice. These suggested that LMO3 is a neuronal-specific oncogene in neuroblastoma, without any rearrangement of the *LMO3* gene (data not shown). However, we failed to establish a stable SH-SY5Y cell line transfected with HEN2. It is presumed that overexpression of HEN2 might have caused cell death or growth arrest in the cells, albeit the reason is elusive.

The double transgenic mice overexpressing LMO2 and TAL1 displayed a more rapid development of leukemia compared with those overexpressing LMO2 alone, suggesting that LMO2 and TAL1 act synergistically through their complex formation in the development of leukemia (13). Of note, Ono et al. reported that LMO2 and TAL1 act as cofactors for GATA3 to induce the expression of the *retinaldehyde dehydrogenase 2* gene in T-cell ALL (39). On the other hand, a stable complex comprising LMO2, TAL1, and GATA1 was required to promote erythroid differentiation (32). Therefore, LMO3 and HEN2 may also form a nuclear complex, including family members of GATA to regulate cell growth and differentiation in neuroblastoma. Our preliminary data have suggested that GATA2, GATA3, GATA4, and GATA6 are highly expressed in neuroblastoma cell lines, among which GATA4 and GATA6 are predominantly coexpressed in neuroblastoma cell lines compared with T-cell ALL lines. Thus, LMO3 and HEN2, in collaboration with GATA and Ldb families, may play a role in determining cell fate in both neural development and neuroblastoma genesis, although this hypothesis needs to be elucidated. Recently, it has been shown that LMO3 enhanced the ability of HEN1 through the physical interaction to transactivate the expression of *Neurogenin-1* as well as *NeuroD* and thereby induced the neuronal differentiation in frog embryos (35). We tested if this is the case in the neuroblastoma cells. However, our preliminary results suggested that the LMO3/HEN2 complex does not transactivate the *Neurogenin-1* as well as *NeuroD* promoter in neuroblastoma cell lines,[5] although it is unclear if the complex could work in normal neuronal development. Thus, like LMO2, alterations in the LMO3-containing transcriptional complex might differentially regulate expression of the downstream target genes closely involved in neuronal differentiation or tumor formation.

[5] Unpublished data.

It is striking that high levels of expression of both *LMO3* and *HEN2* are significantly associated with the poor prognosis in primary neuroblastomas. This clearly reflects how importantly both genes are functioning in the progression of neuroblastoma *in vivo*. Of interest, expression of either gene is well correlated with *MYCN* amplification, raising the possibility that they might be the downstream targets of MYCN. However, we could not confirm it in human neuroblastoma cell line SH-EP in which MYCN was regulated under the control of the rTet-inducible expression system (40). In agreement with this, cDNA microarray-based screening for the genes induced in the *MYCN*-amplified neuroblastoma cells thus far failed to detect either LMO3 or HEN2 (41, 42). The link between LMO family molecules and the other oncogenes or tumor suppressor genes is also important. Despite the lack of prognostic significance, LMO4 overexpressed in breast cancer seems to be indispensable in the mammary carcinogenesis because it interacts with both BRCA1 and CtIP to repress the BRCA1 function (10). This suggests that, similarly to LMO4, LMO3 may also have the interacting partners related to the tumorigenesis. Thus, LMO3 and HEN2 as well as their associated molecules might be good candidates for the future targets of the therapy against aggressive neuroblastomas.

Acknowledgments

Received 12/28/2004; revised 3/9/2005; accepted 3/23/2005.

Grant support: Grant-in-Aid from the Ministry of Health, Labour and Welfare for Third Term Comprehensive Control Research for Cancer, Grant-in-Aid for Scientific Research on Priority Areas from the Ministry of Education, Culture, Sports, Science and Technology, Japan, and Grant-in-Aid for Scientific Research from Japan Society for the Promotion of Science. M. Aoyama is an awardee of the Research Resident Fellowship from the Foundation for Promotion of Cancer Research in Japan.

The costs of publication of this article were defrayed in part by the payment of page charges. This article must therefore be hereby marked *advertisement* in accordance with 18 U.S.C. Section 1734 solely to indicate this fact.

We thank S. Sakiyama for critical reading of the article; A. Morohashi, N. Kitabayashi, H. Murakami, and N. Sugimitsu for excellent technical assistance; and the following institutions and hospitals for supplying the tumor samples: Department of Pediatric Surgery, Iwaki Kyoritsu Hospital; Departments of Pediatrics and Pediatric Surgery, Aichi Medical University; Department of Pediatrics, Nara Hospital; Department of Pediatrics, Kyoto Prefectural University of Medicine; Department of Pediatric Surgery, Kimitsu Central Hospital; Department of Surgery, Gunma Children's Medical Center; Department of Pediatrics, Sapporo National Hospital; Departments of Pediatrics, Pediatric Surgery, and General Surgery, Jichi Medical School; Departments of Pediatrics and Pediatric Surgery, Kagoshima University; Department of Pediatrics, Juntendo University; Department of Pediatric Surgery, Showa University; Department of Pediatric Surgery, Niigata University; Departments of Surgery and Pathology, Chiba Children's Hospital; Department of Pediatric Surgery, Chiba University; Department of Pediatric Surgery, Osaka City General Hospital; Department of Pediatric Surgery, Tsukuba University; Department of Pediatric Surgery, Tokai University; Department of Surgery, Tokyo Metropolitan Kiyose Children's Hospital; Department of Pediatric Surgery, Tohoku University; Tomor Board, Hyogo Prefectural Kobe Children's Hospital; and First Department of Surgery, Hokkaido University.

References

1. Dawid IB, Breen JJ, Toyama R. LIM domains: multiple roles as adaptors and functional modifiers in protein interactions. Trends Genet 1998;14:156–62.
2. Sanchez-Garcia I, Rabbitts TH. The LIM domain: a new structural motif found in zinc-finger-like proteins. Trends Genet 1994;10:315–20.
3. Dawid IB, Toyama R, Taira M. LIM domain proteins. C R Acad Sci III 1995;318:295–306.
4. Rabbitts TH. LMO T-cell translocation oncogenes typify genes activated by chromosomal translocations that alter transcription and developmental processes. Genes Dev 1998;12:2651–7.
5. McGuire EA, Rintoul CE, Sclar GM, Korsmeyer SJ. Thymic overexpression of Ttg-1 in transgenic mice results in T-cell acute lymphoblastic leukemia/lymphoma. Mol Cell Biol 1992;12:4186–96.
6. Fisch P, Boehm T, Lavenir I, et al. T-cell acute lymphoblastic lymphoma induced in transgenic mice by the RBTN1 and RBTN2 LIM-domain genes. Oncogene 1992;7:2389–97.
7. Neale GA, Rehg JE, Goorha RM. Disruption of T-cell differentiation precedes T-cell tumor formation in LMO-2 (rhombotin-2) transgenic mice. Leukemia 1997;3:289–90.
8. Kenny DA, Jurata LW, Saga Y, Gill GN. Identification and characterization of LMO4, an LMO gene with a novel pattern of expression during embryogenesis. Proc Natl Acad Sci U S A 1998;95:11257–62.
9. Visvader JE, Venter D, Hahm K, et al. The LIM domain gene LMO4 inhibits differentiation of mammary epithelial cells *in vitro* and is overexpressed in breast cancer. Proc Natl Acad Sci U S A 2001;98:14452–7.
10. Sum EY, Peng B, Yu X, et al. The LIM domain protein LMO4 interacts with the cofactor CtIP and the tumor suppressor BRCA1 and inhibits BRCA1 activity. J Biol Chem 2002;277:7849–56.
11. Foroni L, Boehm T, White L, et al. The rhombotin gene family encode related LIM-domain proteins whose differing expression suggests multiple roles in mouse development. J Mol Biol 1992;226:747–61.
12. Wadman I, Li J, Bash RO, et al. Specific *in vivo* association between the bHLH and LIM proteins implicated in human T cell leukemia. EMBO J 1994;13:4831–9.
13. Larson RC, Lavenir I, Larson TA, et al. Protein dimerization between Lmo2 (Rbtn2) and Tal1 alters thymocyte development and potentiates T cell tumorigenesis in transgenic mice. EMBO J 1996;15:1021–7.
14. Brown L, Espinosa R III, Le Beau MM, Siciliano MJ, Baer R. HEN1 and HEN2: a subgroup of basic helix-loop-helix genes that are coexpressed in a human neuroblastoma. Proc Natl Acad Sci U S A 1992;89:8492–6.
15. Begley CG, Lipkowitz S, Gobel V, et al. Molecular characterization of NSCL, a gene encoding a helix-loop-helix protein expressed in the developing nervous system. Proc Natl Acad Sci U S A 1992;89:38–42.
16. Brodeur GM, Azar C, Brother M, et al. Effect of genetic factors on prognosis and treatment. Cancer 1992;70:1685–94.
17. Brodeur GM, Nakagawara A. Molecular basis of clinical heterogeneity in neuroblastoma. J Pediatr Hematol Oncol 1992;14:111–6.
18. Brodeur GM, Seeger RC, Schwab M, Varmus HE, Bishop JM. Amplification of N-*myc* in untreated human neuroblastomas correlates with advanced disease stage. Science 1984;224:1121–4.
19. Seeger RC, Brodeur GM, Sather H, et al. Association of multiple copies of the N-*myc* oncogene with rapid progression of neuroblastomas. N Engl J Med 1985;313:1111–6.
20. Nakagawara A, Arima M, Azar CG, Scavarda NJ, Brodeur GM. Inverse relationship between trk expression and N-*myc* amplification in human neuroblastomas. Cancer Res 1992;52:1364–8.
21. Nakagawara A, Arima-Nakagawara M, Scavarda NJ, Azar CG, Cantor AB, Brodeur GM. Association between high levels of expression of the TRK gene and favorable outcome in human neuroblastoma. N Engl J Med 1993;328:847–54.
22. Gross N, Beretta C, Peruisseau G, Jackson D, Simmons D, Beck D. CD44H expression by human neuroblastoma cells: relation to MYCN amplification and lineage differentiation. Cancer Res 1994;54:4238–42.
23. Berwanger B, Hartmann O, Bergmann E, et al. Loss of a FYN-regulated differentiation and growth arrest pathway in advanced stage neuroblastoma. Cancer Cell 2002;2:377–86.
24. Ohira M, Morohashi A, Inuzuka H, et al. Expression profiling and characterization of 4200 genes cloned from primary neuroblastomas: identification of 305 genes differentially expressed between favorable and unfavorable subsets. Oncogene 2003;22:5525–36.
25. Ohira M, Shishikura T, Kawamoto T, et al. Hunting the subset-specific genes of neuroblastoma: expression profiling and differential screening of the full-length-enriched oligo-capping cDNA libraries. Med Pediatr Oncol 2000;35:547–9.
26. Brodeur GM, Pritchard J, Berthold F, et al. Revisions of the international criteria for neuroblastoma diagnosis, staging, and response to treatment. J Clin Oncol 1993;11:1466–77.
27. Matsumura T, Iehara T, Sawada T, Tsuchida Y. Prospective study for establishing the optimal therapy of infantile neuroblastoma in Japan. Med Pediatr Oncol 1998;31:210.
28. Kaneko M, Nishihira H, Mugishima H, et al; Study Group of Japan for Treatment of Advanced Neuroblastoma, Tokyo, Japan. Stratification of treatment of stage 4 neuroblastoma patients based on N-*myc* amplification status. Med Pediatr Oncol 1998;31:1–7.
29. Takihara Y, Tomotsune D, Shirai M, et al. Targeted disruption of the mouse homologue of the *Drosophila* polyhomeotic gene leads to altered anteroposterior patterning and neural crest defects. Development 1997;124:3673–82.
30. Agulnick AD, Taira M, Breen JJ, Tanaka T, Dawid IB, Westphal H. Interactions of the LIM-domain-binding factor Ldb1 with LIM homeodomain proteins. Nature 1996;384:270–2.
31. Jurata LW, Kenny DA, Gill GN. Nuclear LIM interactor, a rhombotin and LIM homeodomain interacting protein, is expressed early in neuronal development. Proc Natl Acad Sci U S A 1996;93:11693–8.
32. Bach I, Carriere C, Ostendorff HP, Andersen B, Rosenfeld MG. A family of LIM domain-associated cofactors confer transcriptional synergism between LIM and Otx homeodomain proteins. Genes Dev 1997;11:1370–80.
33. Osada H, Grutz G, Axelson H, Forster A, Rabbitts TH. Association of erythroid transcription factors: complexes involving the LIM protein RBTN2 and the zinc-finger protein GATA1. Proc Natl Acad Sci U S A 1995;92:9585–9.
34. Valge-Archer VE, Osada H, Warren AJ, et al. The LIM protein RBTN2 and the basic helix-loop-helix protein TAL1 are present in a complex in erythroid cells. Proc Natl Acad Sci U S A 1994;91:8617–21.
35. Bao J, Talmage DA, Role LW, Gautier J. Regulation of neurogenesis by interactions between HEN1 and neuronal LMO proteins. Development 2000;127:425–35.

36. Ono Y, Fukuhara N, Yoshie O. Transcriptional activity of TAL1 in T cell acute lymphoblastic leukemia (T-ALL) requires RBTN1 or -2 and induces TALLA1, a highly specific tumor marker of T-ALL. J Biol Chem 1997;272:4576–81.
37. Aplan PD, Jones CA, Chervinsky DS, et al. An scl gene product lacking the transactivation domain induces bony abnormalities and cooperates with to generate T-cell malignancies in transgenic mice. EMBO J 1997;16:2408–19.
38. Eggert A, Grotzer MA, Ikegaki N, Liu XG, Evans AE, Brodeur GM. Expression of the neurotrophin receptor TrkA down-regulates expression and function of angiogenic stimulators in SH-SY5Y neuroblastoma cells. Cancer Res 2002;62:1802–8.
39. Ono Y, Fukuhara N, Yoshie O. TAL1 and LIM-only proteins synergistically induce retinaldehyde dehydrogenase 2 expression in T-cell acute lymphoblastic leukemia by acting as cofactors for GATA3. Mol Cell Biol 1998;18:6939–50.
40. Lutz W, Stohr M, Schurmann J, Wenzel A, Lohr A, Schwab M. Conditional expression of N-*myc* in human neuroblastoma cells increases expression of α-prothymosin and ornithine decarboxylase and accelerates progression into S-phase early after mitogenic stimulation of quiescent cells. Oncogene 1996;13:803–12.
41. Schuldiner O, Benvenisty N. A DNA microarray screen for genes involved in c-MYC and N-MYC oncogenesis in human tumors. Oncogene 2001;20:4984–94.
42. Shohet JM, Hicks MJ, Plon SE, et al. Minichromosome maintenance protein MCM7 is a direct target of the MYCN transcription factor in neuroblastoma. Cancer Res 2002;62:1123–8.

Clinical significance of serum NM23-H1 protein in neuroblastoma

Junko Okabe-Kado,[1,4] Takashi Kasukabe,[1] Yoshio Honma,[1] Ryoji Hanada,[2] Akira Nakagawara[3] and Yasuhiko Kaneko[1]

[1]Research Institute for Clinical Oncology, Saitama Cancer Center, 818 Komuro, Ina-machi, Kitaadachi-gun, Saitama 362-0806; [2]Saitama Children's Medical Center, 2100 Magome, Iwatsuki, Saitama 339-8551; and [3]Department of Biochemistry, Chiba Cancer Center Research Institute, 666-2 Nitona-cho, Chuo-ku, Chiba 260-8717, Japan

(Received April 28, 2005/Revised July 1, 2005/Accepted July 4, 2005/Online publication August 29, 2005)

We have previously reported that *NM23* genes are overexpressed in various hematological malignancies and that serum NM23-H1 protein levels are useful for predicting patient outcomes. In this study we assessed the clinical implications of serum NM23-H1 protein on neuroblastoma. We examined serum NM23-H1 protein levels in 217 patients with neuroblastoma, including 131 found by mass-screening and 86 found clinically by an enzyme-linked immunosorbent assay, and determined the association between levels of this protein, and known prognostic factors or the clinical outcome. The serum NM23-H1 protein level was higher in neuroblastoma patients than in control children ($P < 0.0001$). Patients with *MYCN* amplification had higher serum NM23-H1 levels than those with a single copy of *MYCN*. Overall survival was assessed in the 86 patients found clinically, and was found to be worse in patients with higher serum NM23-H1 levels (≥ 250 ng/mL) than in those with lower levels (< 250 ng/mL; $P = 0.034$). The higher level of NM23-H1 was correlated with a worse outcome in patients with a single *MYCN* copy, or in those younger than 12 months of age. Serum NM23-H1 protein levels may contribute to predictions of clinical outcome in patients with neuroblastoma. (*Cancer Sci* 2005; 96: 653–660)

The *NM23* gene was identified by differential hybridization of a cDNA library with total RNA extracted from slightly and highly metastatic melanoma cell lines.[1] The *NM23* gene has been identified as a family of genes encoding different isoforms of nucleoside diphosphate kinase (NDPK).[2] *NM23* genes play critical roles in cellular proliferation, differentiation, oncogenesis, and tumor metastasis.[1,3] The mechanisms for these pleiotropic effects are not well understood. Eight isotypes of the human *NM23* gene (*NM23-H1*, *NM23-H2*, *NM23-H3/DR-NM23*, *NM23-H4*, *NM23-H5*, *NM23-H6*, *NM23-H7*, and *NM23-H8*) have been identified.[2] Among these, only *NM23-H1* and *NM23-H2* have been studied extensively in human cancers.

The level of *NM23-H1* expression is inversely correlated with the tumor's metastatic potential in experimental rodent cells and in human tumors such as breast, ovarian, cervical and gastric cancer, hepatocellular carcinoma, and melanomas.[4] Therefore, *NM23-H1* is implicated in the regulation of metastasis in a variety of human cancers. However, overexpression of the *NM23-H1* gene has been reported in various neoplasms including neuroblastoma, hematological malignancies, and pancreatic, lung, ovarian and gastric cancers.[5–8] Overexpression of *NM23-H1* is indicative of a poor patient prognosis for patients with neuroblastoma, acute myelogenous leukemia (AML), or non-Hodgkin's lymphoma (NHL).[8–10]

In neuroblastoma, a gain of 17q is the most frequent genetic abnormality, followed by 1p deletion and *MYCN* amplification, both of which correlate closely with 17q gain. The three genetic events are strong predictors of unfavorable prognosis.[11,12] The *NM23* genes are located at the edge of the common chromosomal region of 17q gain. Godfrid *et al.* identified genes that are activated in the *MYCN* downstream pathway using SAGE libraries of *MYCN*-transfected and control neuroblastoma cell lines.[13] The *NM23-H1* and *NM23-H2* genes are strongly induced in *MYCN*-expressing cells. Neuroblastoma tumor and cell line panels reveal a striking correlation between *MYCN* amplification and mRNA or protein expression of both *NM23* genes. These findings suggest that *NM23-H1* and *NM23-H2* expression may be increased by 17q gain in neuroblastoma, and can be further upregulated by *MYCN* overexpression. These observations suggest a role of *NM23-H1* and *NM23-H2* in the tumorigenesis of an unfavorable type of neuroblastoma.

We previously established an enzyme-linked immunosorbent assay (ELISA) technique for determining the serum level of NM23-H1 protein.[14] Serum levels of NM23-H1 in patients with NHL and AML are significantly higher than those in controls, and elevated NM23-H1 levels correlate with poor prognosis in these patients.[10,15] It has been strongly suggested that serum NM23-H1 protein is produced directly by tumor cells and its level depends on the total mass of malignant cells overexpressing *NM23-H1*.[14,16] These results indicate that the serum level of NM23-H1 protein may be clinically useful as a prognostic factor in NHL and AML. The present study assessed the clinical implications of serum NM23-H1 protein levels in patients with neuroblastoma, in whom tumor samples were used to determine the biological prognostic factors.

Materials and Methods

Patients and controls

Serum NM23-H1 protein was measured in 217 untreated neuroblastoma patients who were admitted to various institutions in Japan and underwent biopsy or surgery between 2000 and 2002. The 217 patients included 131 who were found by

*To whom correspondence should be addressed.
E-mail: jkado@cancer-c.pref.saitama.jp

 doi: 10.1111/j.1349-7006.2005.00091.x

a mass-screening (MS) program for infants at 6 months of age by measuring urinary catecholamine metabolites and 86 who were found clinically.[17] Of the 86 patients, 29 who were younger than 12 months old were mostly found before MS, and 57 who were 12 months old or older underwent MS with a negative result, or did not undergo MS. Patients were staged according to the International Neuroblastoma Staging System (INSS).[18] Patients of any age with stage 1 or 2 disease, and those younger than 12 months of age with stage 3 disease were treated by surgery or surgery and chemotherapy consisting of cyclophosphamide and vincristine; patients 12 months or older with stage 3 or stage 4 disease and those younger than 12 months of age with stage 4 disease were treated according to the protocol published by the Japanese Neuroblastoma Study Group.[19] Serum samples from 23 children consisting of 22 with inguinal hernias and one with an edematous scrotum before surgery were analyzed for comparison. The median age of the children was 23 months (range: 3–49 months). Informed consent was obtained from patients and/or their parents, and the ethics committee of Saitama Cancer Center approved the study design.

Venous blood samples

Peripheral venous blood samples were collected in sterile test tubes with heparin and placed on ice. The samples were centrifuged at 2000*g* for 15 min at 4°C, and stored at −20°C. As a marker of hemolysis, free serum hemoglobin (Hb) was determined according to the method of Testa *et al.*[20]

ELISA for human NM23-H1 protein

NM23-H1 protein levels in serum were determined using a sandwich ELISA assay, as described previously.[14,15] Recombinant NM23-H1-GST protein was used as a standard.

Examination of *MYCN* copy number, TRKA expression and ploidy

DNA preparation, digestion, and Southern blot analysis using the *MYCN* probe were carried out as described previously.[12] The presence of more than three copies of the *MYCN* gene per haploid genome was considered to indicate amplification.[21] *TRKA* expression was examined by northern blotting as reported previously.[22] DNA index was analyzed on a Becton-Dickinson FACScan flow cytometer by DNA cell-cycle analysis software (version C).

Statistical analysis

The significance of differences in various clinical and biological aspects of the disease among the patient groups was examined by using the Mann–Whitney *U* or Kruskal–Wallis test (non-parametric analysis). Spearman's correlation coefficient (rs) by ranks was used to evaluate the correlation between paired values. Survival analysis was performed according to the Kaplan–Meier method, and the significance of differences in survival was determined by using the generalized Wilcoxon's and log-rank tests. A multivariate analysis of prognostic factors was performed using Cox's proportional-hazards regression model. All statistical analyses were performed with Excell Statcel and Stat Flex software (version 5.0, Artech Co. Ltd, Osaka, Japan), and $P < 0.05$ was taken to indicate significance.

Results

Examination of serum NM23-H1 protein levels in neuroblastoma patients and control children

The serum level of NM23-H1 was examined in 217 neuroblastoma patients and 23 control children. The serum levels of NM23-H1 were significantly higher in patients with neuroblastoma ($n = 217$, mean ± SD 176 ± 280 ng/mL) than in the control children ($n = 23$, 27 ± 41 ng/mL, $P < 0.0001$; Fig. 1a). The serum NM23-H1 levels of the control children were higher than those of the healthy adults (data not shown). The serum NM23-H1 levels in patients with neuroblastoma were significantly higher than those in patients with various hematological malignancies (data not shown). Next, the relationship between serum levels of NM23-H1 and Hb was examined in 217 neuroblastoma patients and 23 control children, because the NM23-H1 protein leaked from red blood cells by hemolysis may have elevated the serum NM23-H1 levels.[23] The results showed a weak correlation (rs = 0.3958, $P = 7.5356 \times 10^{-10}$, Spearman's correlation coefficient by ranks), although some patients had a higher Hb level but a lower NM23-H1 level, or a lower Hb level but a higher NM23-H1 level (Fig. 1b). When we chose samples from 156 patients

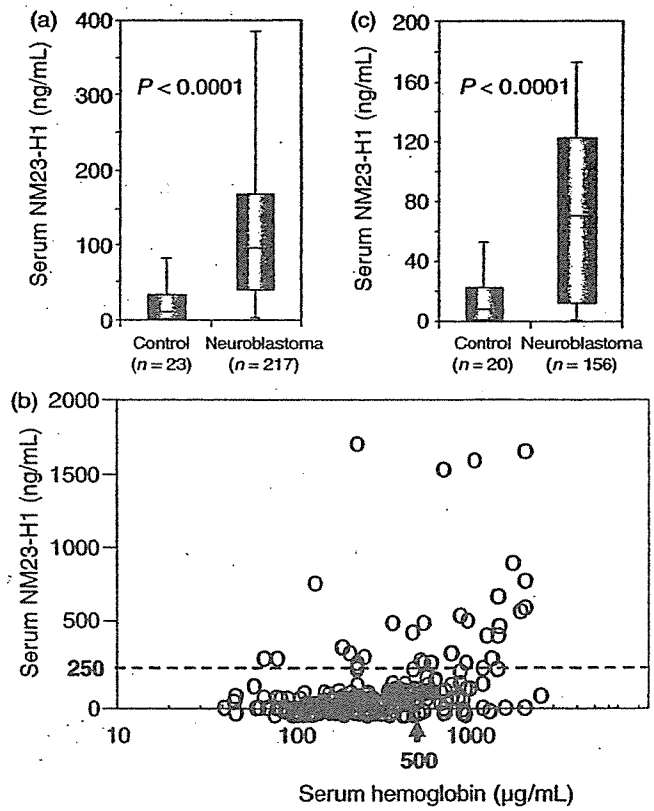

Fig. 1. Serum NM23-H1 levels in patients with neuroblastoma and in control children. (a) Box plots of NM23-H1 serum levels for 217 patients with neuroblastoma and 23 control children with any serum hemoglobin levels. (b) Relationship between the serum levels of NM23-H1 and hemoglobin in all samples examined (black circles, neuroblastoma patients [$n = 217$]; red circles, control children [$n = 23$]). (c) Box plots of NM23-H1 serum levels for 156 patients with neuroblastoma and 20 control children with serum hemoglobin levels less than 500 μg/mL.

 doi: 10.1111/j.1349-7006.2005.00091.x

Table 1. Relationship between serum NM23-H1 protein levels and clinicopathological findings in 217 patients with neuroblastoma and 23 control children

Clinicopathological findings	Number of patients (mean ± SD)	Serum NM23-H1 (ng/mL)	*P*-value (analysis)
Control children	23	27 ± 41	
All patients	217	176 ± 280	< 0.0001 (MW)
Method of detection			
Mass-screening	131	135 ± 206	
Found clinically	86†	239 ± 357	0.0595 (MW)
Age of patients			
< 12 months	134	168 ± 292	
≥ 12 months	83	190 ± 260	0.2427 (MW)
Stage of the disease			
1 + 2 + 4s	122	136 ± 159	
3 + 4	95	227 ± 378	0.8088 (MW)
Primary site			
Mediastinum	31	145 ± 212	
Adrenal	101	187 ± 290	
Abdomen	78	184 ± 302	0.3393 (KW)
Others	7	74 ± 82	
MYCN copy number			
1	186	143 ± 204	
> 3	31	378 ± 519	0.0006 (MW)
TRKA expression	173		
Medium or high	125	150 ± 209	
None or low	48	238 ± 373	0.4629 (MW)
Ploidy	168		
Diploid	69	188 ± 273	
Hyperdiploid	99	185 ± 284	0.9012 (MW)
Others	7	112 ± 126	

MW, Mann–Whitney *U*-test; KW, Kruskal–Wallis test. †Table 2.

and 20 control children with serum Hb less than 500 μg/mL, the correlation between serum NM23-H1 and Hb levels was negligible (rs = 0.2351, $P = 0.0035$). Even in these patients, the serum levels of NM23-H1 were significantly higher ($n = 156$, 113 ± 184 ng/mL) than in the control children ($n = 20$, 20 ± 35 ng/mL, $P < 0.0001$; Fig. 1c).

Relationship between serum NM23-H1 protein levels and clinicopathological features in neuroblastoma

The relationship between serum NM23-H1 levels and various clinical and biological features in the 217 patients is shown in Table 1. The serum NM23-H1 levels tended to be higher in patients found clinically than in those found by MS ($P = 0.0595$), and were significantly higher in patients with amplified *MYCN* copies than in those with a single *MYCN* copy ($P = 0.0006$; Table 1). There was a correlation between *MYCN* amplification and the elevated serum NM23-H1 level (≥ 250 ng/mL) in all 217 patients (rs = 0.6970, $P = 0.0005$). However, serum Hb concentrations did not correlate with *MYCN* amplification ($P = 0.6320$), or other factors (data not shown). There was no significant difference in the serum NM23-H1 levels between two groups of patients classified by age of the patients, stage of the disease, expression levels of *TRKA*, or tumor cell ploidy (Table 1).

Serum NM23-H1 levels and overall survival

Of the 217 patients, the 86 patients who were found clinically were included and the 131 patients found by MS were excluded from survival analysis, because all the 131 patients were alive at the last follow-up (18–51 months), and the clinical and biological features are different for the patients found by MS and those found clinically.[12] The relationship between serum NM23-H1 levels and various clinical and biological features in the 86 patients was similar to that found for all 217 patients (Tables 1, 2). The 86 patients were divided into two groups according to various cut-off points over 100 ng/mL, which was the upper limit in control serum (mean + 2 × SD = 20 + 2 × 35 = 90). The cut-off points used here were 100 ng/mL (< 100, $n = 39$, *vs* ≥ 100, $n = 47$), 150 ng/mL (< 150, $n = 54$, *vs* ≥ 150, $n = 32$), 200 ng/mL (< 200, $n = 60$, *vs* ≥ 200, $n = 26$) and 250 ng/mL (< 250, $n = 64$, *vs* ≥ 250, $n = 22$). The cut-off value of greater than 250 ng/mL showed the most significant prognostic effects with generalized Wilcoxon's and log-rank test analysis (data not shown). Therefore, we used 250 ng/mL of serum NM23-H1 as a cut-off value. As shown in Figure 2a, patients with the higher serum NM23-H1 levels had worse overall survival than those with the lower levels ($P = 0.0219$ according to the generalized Wilcoxon test, $P = 0.0340$ according to the log-rank test). Overall survival was significantly worse for patients who were 12 months or older than for those younger than 12 months of age ($P = 0.0364$ and $P = 0.0158$), for patients at stages 3 and 4 than for those at stages 1, 2 and 4S ($P = 0.0157$ and $P = 0.0082$), and for patients with *MYCN* amplification than for those with a single copy of *MYCN* ($P = 0.0195$ and $P = 0.0054$; Fig. 2b,c,d). These results